The OsSRO1c-OsDREB2B complex undergoes protein phase transition to enhance cold tolerance in rice

Dan Hu, Yilong Yao, Yan Lv, Jun You, Yu Zhang, Qingya Lv, Jiawei Li, Stephanie Hutin, Haiyan Xiong, Chloe Zubieta, et al.

The OsSRO1c-OsDREB2B complex confers cold tolerance via protein phase transition and regulation of *COLD1* in rice

Dan Hu[1], Yilong Yao[1], Yan Lv[1,3], Jun You[1,3], Qingya Lv[1], Jiawei Li[1], Stephanie Hutin[2], Haiyan Xiong[1], Chloe Zubieta[2], Xuelei Lai[1*] and Lizhong Xiong[1*]

[1]National Key Laboratory of Crop Genetic Improvement, Hubei Hongshan Laboratory, Huazhong Agricultural University, Wuhan, China.

[2]Laboratoire de Physiologie Cellulaire et Végétale, Université Grenoble-Alpes, CNRS, CEA, INRAE, IRIG-DBSCI, 38000 Grenoble, France.

[3]Current address: Key Laboratory of Biology and Genetic Improvement of Oil Crops, Ministry of Agriculture, Oil Crops Research Institute of the Chinese Academy of Agricultural Sciences, Wuhan, China.

*Correspondence: xuelei_lai@mail.hzau.edu.cn (Xuelei Lai), lizhongx@mail.hzau.edu.cn (Lizhong Xiong)

Abstract

Cold stress is one of the major abiotic stress factors affecting rice growth and development, leading to significant yield loss in the context of global climate change. Exploring natural variants that confer cold resistance and the underlying molecular mechanism responsible for this is the major strategy to breed cold tolerant rice varieties. Here, we show that the natural variations of a *SIMILAR to RCD ONE (SRO)* gene, *OsSRO1c*, confer cold tolerance in rice at both seedling and booting stages. OsSRO1c possesses intrinsic liquid-liquid phase separation ability *in vivo* and *in vitro* and recruits an AP2/ERF transcription factor and cold stress positive regulator, OsDREB2B, into its biomolecular condensates in the nucleus, resulting in elevated transcriptional activity of OsDREB2B. The OsSRO1c-OsDREB2B complex directly responds to low temperature through dynamic phase transitions and regulates key cold response genes, including *COLD1*. Furthermore, introgression of an elite haplotype of *OsSRO1c* into a cold susceptible *indica* rice significantly increases its cold resistance ability. Thus, our work reveals a novel cold stress regulation module and provides a promising gene resource for breeding cold tolerant rice varieties.

Key words: cold stress sensing, natural variation, crop genetic improvement, liquid-liquid phase separation, climate change

Introduction

Rice (*Oryza sativa* L.) is one of the most important staple food crops in the world, mainly distributed in the tropical and temperate zones, and is very sensitive to even small changes in temperature and is particularly susceptible to cold stress (Huang et al., 2012; Wang et al., 2018). Global climate change has caused more frequent occurrence of extreme temperature conditions, thus the study of the mechanism of temperature sensing in plants and the exploration of potential temperature sensors is key for the genetic improvement of temperature adaptation in crop plants (Hayes et al., 2021; Ding and Yang, 2022; Noguchi and Kodama, 2022). Recent studies in the model dicot, *Arabidopsis thaliana*, suggested that liquid-liquid phase separation (LLPS) may be a novel mechanism for environmental signal sensing, including temperature sensing (Li and Fang, 2020; Jung et al., 2023; Kerbler and Philip, 2023). For example, EARLY FLOWERING 3 (ELF3) with a prion-like domain forms liquid droplets in response to increasing ambient temperatures and act as a thermosensor in Arabidopsis (Jung et al., 2020; Silva et al., 2020; Hutin et al., 2023). During vernalization, FRIGIDA (FRI) forms nuclear condensates under cold exposure thereby reducing its occupancy at the promoter of *FLOWERING LOCUS C* (*FLC*), a key floral repressor, leading to timely vegetative growth to reproductive growth transition in response to seasonal temperature changes in Arabidopsis (Zhu et al., 2021). However, thermosensors and the underlying mechanisms, including ambient temperature sensing and stress temperature sensing (cold and heat stresses), in crop plants are still largely unknown, particularly in important crop species such as rice.

Cold stress, one of the major abiotic stress factors, can severely affect rice growth and development, including germination and seedling and booting stages, resulting in serious yield losses (Lu et al., 2014; Zhu, 2016; Li et al., 2022; Soualiou et al., 2022; Zhang et al., 2022). Searching for superior alleles for cold tolerance by dissecting natural variations is a major approach for breeding cold tolerant rice varieties. This led

to the identification of key cold tolerance genes, such as *CHILLING TOLERANCE DIVERGENCE 1* (*COLD1*) (Ma et al., 2015), Cold Tolerance at Booting stage 4a (*CTB4a*) (Zhang et al., 2017) and *Chilling Tolerance 1* (*HAN1*) (Mao et al., 2019) identified through QTL mapping, *bZIP73* (Liu et al., 2018) identified through association analyses using unlinked amino-acid variations markers*, OsMYB2* (Lv et al., 2016) and *SEC13 Homolog 1 (OsSEH1)* (Gu et al., 2023) identified through genome-wide association study (GWAS).

Deciphering the regulatory network controlling the expression of cold tolerance genes is an important challenge in developing cold tolerant rice varieties. One family of putative regulatory proteins affecting cold tolerance gene expression is the SIMILAR to RCD ONE (SRO) protein family. The SROs are a class of plant-specific proteins that are involved in response to a variety of abiotic stresses such as oxidative, drought, cold and salinity stresses (You et al., 2013; Liu et al., 2014; You et al., 2014; Gao et al., 2022; Wang et al., 2022). SROs have a poly(ADP-ribose) polymerase (PARP) domain and a C-terminal RCD1 (Radical-induced Cell Death1)-SRO-TAF4 (TATA-Box Binding Protein Associated Factor 4) domain (RST) (Jaspers et al., 2009; Jaspers et al., 2010). The RST domain has an αα-hairpin super-secondary motif, also named αα-hubs that is responsible for mediating interactions with multiple different families of transcription factors (Jaspers *et al.*, 2010; Bugge et al., 2018). In earlier studies, SROs were thought to have no poly(ADP-ribose) polymerase activity due to the lack of catalytic HYE residues in the PARP domain (Jaspers *et al.*, 2010). But in later studies, a wheat SRO member TaSRO1 shows poly(ADP-ribose) polymerase activity *in vitro* (Liu *et al.*, 2014). In addition, the Arabidopsis SRO2 and the maize ZmSRO1d are reported to mediate the mono-ADP-ribosylation of Salt-inducible Zinc Finger (SZF) proteins and ZmRBOHC that are involved in plant immunity and drought resistance, respectively (Kong et al., 2021; Gao *et al.*, 2022). These studies suggest that while some SRO proteins may catalyze poly/mono-ADP-ribosylation of a substrate protein, other SRO

proteins with little or no poly(ADP)-ribosylation activity may interact with or recruit transcription factors and participate in abiotic stress response.

In this study, we identified that the natural variation of *OsSRO1c* conferred cold tolerance in rice at both seedling and booting stages. Introducing an elite *OsSRO1c* haplotype into a cold sensitive rice variety significantly increased its cold resistance ability, suggesting that *OsSRO1c* has strong potential in breeding applications. In order to determine the mechanism of action of OsSRO1c, we performed *in vitro* biochemical and *in vivo* genetic studies. We found that while OsSRO1c exhibits little enzymatic poly(ADP)ribosylation activity, OsSRO1c physically interacts with OsDREB2B, an AP2/ERF transcription factor and positive regulator of cold response. OsSRO1c possesses intrinsic LLPS ability and recruits OsDREB2B into nuclear bodies to facilitate its transcriptional activity. Furthermore, the OsSRO1c-OsDREB2B complex could directly respond to low temperature through dynamic phase transitions, suggesting a possible mechanism for conferring cold tolerance via transcriptional regulation of key cold tolerance genes and targets of OsDREB2B, including *COLD1*.

Results

OsSRO1c is associated with cold tolerance in rice

In our previous study, we found that a member of the SRO family, OsSRO1c, participates in multiple abiotic stress responses, including cold stress (You *et al.*, 2013; You *et al.*, 2014). In this study, we sought to identify superior natural variations for cold stress and investigate the underlying molecular mechanism of *OsSRO1c* in cold stress responses. Firstly, we conducted a candidate gene association analysis for *OsSRO1c* using our previous GWAS data of cold tolerance of rice seedling (Lv *et al.*, 2016). A total of 106 single nucleotide polymorphisms (SNPs) within the *OsSRO1c* locus were identified (Supplementary Table 1). Among them, two non-synonymous variants (SNP4361 and SNP5727) were significantly associated with changes in electrolyte leakage after recovery for 7 d (ELR, a major parameter of susceptibility to cold) ($P <$

10^{-2}), and showed almost complete linkage disequilibrium (LD, $r^2 = 0.99$) (Fig. 1a). SNP4361 corresponded to an R32S mutation in the WWE domain, while SNP5727 resulted in a P377L mutation close to the PARP domain (Fig. 1b). We then performed haplotype analysis based on the two SNPs and classified the 527 rice germplasms (the collection used in the GWAS analysis (Lv *et al.*, 2016)) into two haplotype groups (*OsSRO1c*^{Hap1} and *OsSRO1c*^{Hap2}). Among the association mapping population, 355 germplasms carry *OsSRO1c*^{Hap1}, consisting of 53.80% *Indica* (Ind), 42.82% *Japonica* (Jap), and 3.38% intermediate (Inter), while the remaining 172 germplasms carry *OsSRO1c*^{Hap2}, consisting of 60.47% Ind, 26.74% Aus, and 11.63% Inter, but only 1.16% Jap (Fig. 1c). *OsSRO1c*^{Hap1} varieties exhibited lower ELR and a higher survival rate than *OsSRO1c*^{Hap2} after natural chilling stress in both the whole population and the *indica* subpopulation (Fig. 1d and Extended Data Fig. 1). Next, we analyzed the geographical distribution of the two haplotypes using 820 rice germplasms collected from China (Zhao et al., 2021). We found that *OsSRO1c*^{Hap1} varieties were far more than *OsSRO1c*^{Hap2} varieties and were distributed in low temperature regions at high latitudes (Extended Data Fig. 2), suggesting that *OsSRO1c*^{Hap1} may be a superior haplotype for cold tolerance. In addition, we performed phylogenetic, population differentiation (F_{ST}) and nucleotide diversity (π) analysis. Phylogenetic analysis using 527 *O. sativa* accessions showed that the two alleles have diverged between *indica* and *japonica* subspecies (Extended Data Fig. 3a). Next, we conducted sequence diversity analysis on the 150-kb genomic region around *OsSRO1c* using the same population. Population differentiation (F_{ST}) analysis indicates a large differentiation of *OsSRO1c* between *indica* and *japonica* (Extended Data Fig. 3b). Nucleotide diversity (π) at the *OsSRO1c* locus in *japonica* accessions was significantly lower than that in the *indica* accessions (Extended Data Fig. 3c). Taken together, our genetic analysis suggests that *OsSRO1c* is significantly associated with cold tolerance in rice.

OsSRO1c positively regulates cold response in rice and shows high potential in breeding cold tolerance rice

To investigate the function of *OsSRO1c* in cold response, we generated *ossro1c* knockout mutants (*1c*-CR) by CRISPR/Cas9-based mutagenesis in the wild type (WT) ZH11 background, which contains *OsSRO1c*^{Hap1} allele. Three independent lines (*1c*-CR-8, *1c*-CR-10, and *1c*-CR-14) were used for subsequent studies (Extended Data Fig. 4a). Rice seedlings were treated at 4℃ for 3 d and set for recovery at normal growth conditions for 7 d, the mutant lines displayed more sensitivity to cold than the WT ZH11 (Fig. 1e,f). Consistent with the cold sensitive phenotypes, we found that the mutant lines exhibited higher electrolyte leakage compared with WT seedlings during cold treatment, indicating that their membrane integrity is more affected (Fig. 1g). Next, we generated transgenic plants using the *OsSRO1c* native promoter to drive the two haplotypes in the *1c*-CR mutant background (named Com^{Hap1} and Com^{Hap2}, respectively). The reduced survival rate and increased electrolyte leakage of *1c*-CR after cold treatment were restored to WT levels by *1c-CR* lines complemented with *OsSRO1c*^{Hap1} but not *OsSRO1c*^{Hap2} (Extended Data Fig. 4b-d), suggesting that *OsSRO1c*^{Hap1} is a superior allele in conferring cold tolerance. Furthermore, we generated overexpression (OE) lines of *OsSRO1c*^{Hap1} and *OsSRO1c*^{Hap2}, respectively, under the control of a maize *ubiquitin* gene promoter, in the WT background (named OE^{Hap1} and OE^{Hap2}, respectively) (Extended Data Fig. 4e). After cold stress treatment, OE^{Hap1} significantly improved the survival rate, while OE^{Hap2} has no significant difference in survival rate compared with WT (Extended Data Fig. 4f,g). Interestingly, both OE lines showed significantly decreased electrolyte leakage than WT ZH11, with *OsSRO1c*^{Hap1} exhibiting the lowest ELR (Extended Data Fig. 4h). These results indicate that OsSRO1c is a positive regulator for cold tolerance in rice and that the *OsSRO1c*^{Hap1} allele confers increased cold tolerance versus the *OsSRO1c*^{Hap2} allele.

Next, we asked whether the elite allele *OsSRO1c*^{Hap1} has breeding value in rice cold tolerance improvement. To this end, we generated a near-isogenic line (NIL-*OsSRO1c*^{Hap1}) by introducing the *OsSRO1c*^{Hap1} allele from cultivar OM1723 into Guichao#2, a cold susceptible *indica* rice that used to be widely cultivated in southern China, to replace its *OsSRO1c*^{Hap2} allele. We evaluated the cold tolerance at four-leaf seedling and booting stages and found that the corresponding survival rate and relative seed setting rate were both significantly improved in the NIL-*OsSRO1c*^{Hap1} compared with Guichao#2 (Fig. 1h,i), suggesting that the *OsSRO1c*^{Hap1} allele is highly valuable in breeding cold tolerant rice varieties.

Both OsSRO1c variants interact with OsDREB2B, a positive regulator in cold tolerance in rice

To further dissect the underlying molecular mechanism of *OsSRO1c* in cold tolerance, we focused on the interacting proteins of OsSRO1c that we previously screened via yeast two-hybrid (Y2H) (You *et al.*, 2013). Among the interacting proteins, we chose the transcription factor OsDREB2B for further study as it was reported to be involved in multiple abiotic stress responses, such as drought and heat (Chen et al., 2008; Matsukura et al., 2010). However, whether *OsDREB2B* is involved in the cold response is unknown. Considering that the SNP variation of *OsSRO1c* caused amino acid changes, the interaction between OsSRO1c variants and OsDREB2B was tested through pull-down assays (Fig. 2a) and co-immunoprecipitation (Co-IP) experiments (Fig. 2b), confirming the interaction was preserved for all variants. We further verified the interaction using a luciferase complementation assay in *N. benthamiana* tobacco leaves (Fig. 2c) and bimolecular fluorescence complementation (BiFC) assays in rice protoplasts (Fig. 2d). Together, these *in vitro* and *in vivo* experiments demonstrate that both OsSRO1c variants interact with OsDREB2B.

Next, we generated *osdreb2b* mutant lines (*2b*-CR) by CRISPR/Cas9 and overexpression lines (*2B*-OE) under the control of the maize *ubiquitin* promoter. Three

independent mutant lines (*2b*-CR-1, *2b*-CR-12, and *2b*-CR-42) and OE lines (*2B*-OE-6, *2B*-OE-14 and *2B*-OE-34) were used for further analysis (Extended Data Fig. 5). The *osdreb2b* mutant seedlings were more sensitive to cold stress than WT ZH11 (Fig. 2e,f). Consistently, the leaf electrolyte leakage increased more rapidly in the seedlings of the loss-of-function mutant lines than WT ZH11 during cold stress treatment (Fig. 2g). In contrast, the survival rates were significantly higher in the OE seedlings compared with the WT, and the leaf electrolyte leakage was significantly lower in the OE seedlings (Fig. 2h-j). Taken together, these results indicated that OsDREB2B is a positive regulator in cold tolerance in rice.

OsSRO1c^{Haps}-OsDREB2B complexes form distinct condensates that modulate OsDREB2B activity

While analyzing the BiFC assays in rice protoplasts, we observed that the fluorescence signal of the OsSRO1c-OsDREB2B complex showed a granular structure rather than a disperse distribution in the nucleus under both normal and cold stress conditions (Fig. 2d and Extended Data Fig. 6). This led us to speculate that the OsSRO1c-OsDREB2B complex may form condensates in the nucleus and this may have an effect on activity. Interestingly, we found that under normal conditions, the average puncta area of OsSRO1c^{Hap1}-OsDREB2B complex was larger than OsSRO1c^{Hap2}-OsDREB2B complex, while the puncta number was less for the OsSRO1c^{Hap1}-OsDREB2B complex, (Extended Data Fig. 7), suggesting that the puncta formed by the two complexes may possess distinct properties. We further characterized the granules formed by the two complexes in *N. benthamiana* leaves. Both of the complexes showed a single large condensate in the nucleus under room temperature conditions but turned into smaller granules upon cold treatment (Fig. 3a). The relative area of the condensate to the whole nucleus was larger for the OsSRO1c^{Hap1}-OsDREB2B complex than the OsSRO1c^{Hap2}-OsDREB2B complex under room temperature condition (Fig. 3b). After cold stress, the average puncta area and puncta number for the OsSRO1c^{Hap1}-OsDREB2B complex was

larger and less in number than the OsSRO1c^{Hap2}-OsDREB2B complex (Fig. 3c,d), respectively, in agreement with the BiFC results in rice protoplasts (Fig. 2d and Extended Data Fig. 7a,b). We further examined the fluidity of granules of the two complexes using fluorescence recovery after photobleaching (FRAP) and found that the fluorescence of both complexes showed partial yet rapid recovery within 60 s after photobleaching under cold conditions, but not under room temperature conditions, indicating that these granules are highly dynamic under cold stress but not at room temperature conditions (Fig. 3e and Extended Data Fig. 8). We also found that the FRAP signal recovery of the OsSRO1c^{Hap1}-OsDREB2B complex was faster than that of the OsSRO1c^{Hap2}-OsDREB2B complex in cold conditions, suggesting that the granules formed by OsSRO1c^{Hap1}-OsDREB2B complex are more dynamic (Extended Data Fig. 8). Furthermore, since OsDREB2B is a member of the AP2/ERF transcription factor family, we wondered whether the observed different dynamics of the OsSRO1c^{Haps}-OsDREB2B complexes could fine-tune the transcriptional activity of OsDREB2B. Indeed, co-transfection of OsSRO1c^{Hap1} and OsDREB2B in rice protoplasts promote the transcriptional activity of OsDREB2B under both room temperature and cold stress conditions, while co-transfection of OsSRO1c^{Hap2} and OsDREB2B showed no effect or slightly decreased transcriptional activity of OsDREB2B under room temperature and cold conditions, respectively (Fig. 3f). Taken together, these data suggested that both OsSRO1c variants co-condense with OsDREB2B via liquid-liquid phase separation (LLPS) with distinct dynamics, but only OsSRO1c^{Hap1} could promote the transcriptional activity of OsDREB2B.

OsSRO1c undergoes LLPS *in vivo* and *in vitro*

Since the OsSRO1c-OsDREB2B complex could form macromolecular condensates, we sought to understand which of the two proteins in the complex played a major role for the condensate formation. As *OsSRO1c^{Hap1}* exhibited the most effects on cold tolerance, we focused on this allele. We generated transgenic lines to constitutively express *GFP*-

252 *OsSRO1c*^{Hap1} or *GFP-OsDREB2B* in the WT ZH11 background and found that
253 OsSRO1c^{Hap1}, but not OsDREB2B, showed granule-like structures in root-tip nuclei
254 under both normal and cold stress conditions (Fig. 4a Extended Data Fig. 9). To further
255 confirm this result, we expressed *GFP-OsSRO1c*^{Hap1} or *GFP-OsDREB2B* in rice
256 protoplasts and *N. benthamiana* leaves. We found that OsSRO1c^{Hap1} exhibited punctate
257 structures in both systems, whereas OsDREB2B was uniformly distributed in both
258 systems (Fig. 4b,c). We then examined the fluidity of OsSRO1c^{Hap1} granules using
259 FRAP assays and found that its fluorescent intensity rapidly recovered within 60 s after
260 photobleaching, indicating that OsSRO1c^{Hap1} granules are dynamic protein liquid
261 droplets (Fig. 4d). Next, we investigated the LLPS behavior of OsSRO1c^{Hap1} protein *in*
262 *vitro*. The purified GFP-OsSRO1c^{Hap1} protein formed liquid droplets upon the addition
263 of the crowding agent polyethylene glycol 6000. In contrast, both GFP-OsDREB2B
264 and GFP protein failed to produce liquid droplets under the same conditions (Fig. 4e
265 and Extended Data Fig. 10). FRAP experiments showed that the fluorescence signal
266 within the droplet of GFP-OsSRO1c^{Hap1} recovered rapidly after photobleaching,
267 suggesting that GFP-OsSRO1c^{Hap1} droplets are highly dynamic *in vitro* (Fig. 4f)
268 Together, these experiments demonstrate that OsSRO1c^{Hap1} undergoes LLPS *in vivo*
269 and *in vitro*.
270 Next, we sought to understand the driving force of the LLPS behavior of OsSRO1c^{Hap1}.
271 As intrinsically disordered regions (IDR) are often associated with LLPS, we examined
272 the protein sequence and identified residues 115-187 as the main IDR (Fig. 4g). We
273 constructed the IDR fragment and IDR truncated version of OsSRO1c^{Hap1} (ΔIDR) and
274 examined their LLPS behavior in tobacco leaves (Fig. 4h). The IDR fragment formed
275 larger condensate-like structures than the full-length OsSRO1c^{Hap1}, while the ΔIDR
276 showed a diffuse signal in the nucleus (Fig. 4h), suggesting that the IDR is key for
277 OsSRO1c^{Hap1}'s LLPS behavior. Furthermore, amino acid composition analysis of the
278 IDR showed that negatively charged glutamic acid (E) and positively charged arginine
279 (R) are over-represented (14 and 12, respectively). We constructed two OsSRO1c^{Hap1}

variants by mutating these residues to Ala (14EmA and 12RmA, respectively) and examined their LLPS behavior in tobacco leaves (Fig. 4h). We found that 12RmA showed complete diffusion in the nucleus and that part of the 14EmA proteins localized to the nucleolus with the remaining proteins in the nucleus showing a dispersed distribution (Fig. 4h), suggesting that the charged residues in the IDR are key for droplet formation of the OsSRO1c. Thus, it is likely that electrostatic forces are the driving force for the LLPS behavior of OsSRO1c.

Since liquid droplet formation between OsSRO1c^{Hap1} and OsDREB2B promoted the transcriptional activity of OsDREB2B, we sought to determine the effect of the OsSRO1c^{Hap1} IDR variants on the transcriptional activity of OsDREB2B. We first performed BiFC assays of IDR, ΔIDR, 14EmA, and 12RmA with OsDREB2B in tobacco leaves, and found that all these variants retained their physical interaction with OsDREB2B (Fig. 4i). However, variants whose LLPS ability was weakened or completely abolished, including ΔIDR, 14EmA and 12RmA, had no effect on the transcriptional activities of OsDREB2B in both room temperature and cold conditions (Fig. 4j). In contrast, the OsSRO1c^{Hap1}-full length or the OsSRO1c^{Hap1}-IDR alone that can co-condense with OsDREB2B significantly promote OsDREB2B transcriptional activities under both room temperature and cold conditions (Fig. 4j). To further determine whether OsSRO1c^{Hap1} regulates the transcriptional activity of OsDREB2B through IDR-mediated LLPS, we performed IDR swap assays using the IDR of reported phase separation proteins, FUS (Patel et al., 2015), MED19a (Cheng et al., 2022) and H2B.8 (Buttress et al., 2022). We found that these recombinant OsSRO1c^{Hap1} chimeric variant proteins remained in the condensed state and promoted the transcriptional activity of OsDREB2B (Extended Data Fig. 11). Taken together, these results demonstrate that the charged residues within the IDR drive the LLPS of OsSRO1c^{Hap1} and that OsSRO1c^{Hap1} promotes the transcriptional activity of OsDREB2B through forming co-condensates via LLPS.

Both natural variations are essential for the function of OsSRO1c

Next, we performed *in vivo* and *in vitro* experiments and confirmed that OsSRO1c^{Hap2} can also undergo LLPS (Extended Data Fig. 12). Since the LLPS formation of OsSRO1c^{Hap1} is primarily determined by the IDR (Fig. 4g-h), while SNP variants are not located in the IDR, we sought to investigate whether SNP variants affect LLPS behavior in OsSRO1c variants. We found that the SNP5727 variation led to a more significant reduction in the average puncta area than that of SNP4361 in both rice protoplast and tobacco system (Extended Data Fig. 13a-d). In addition, we found that individual OsSRO1c variants caused by SNPs retained interaction with OsDREB2B (Extended Data Fig. 13e). We further examined the effect of each SNP mutation on the transcriptional activity of OsDREB2B. The results showed that SNP4361 altered the effect of OsSRO1c on OsDREB2B transcriptional activity from a significant promotion to no significant effect under both normal and cold stress conditions, while the variation of SNP5727 significantly inhibited the transcriptional activity of OsDREB2B under normal conditions but had no significant effect in cold conditions (Extended Data Fig. 13f). Furthermore, we examined the enzyme activity of the OsSRO1c variants and their effect on the protein stability of OsDREB2B. These results suggested that the OsSRO1c variants did not differ in terms of enzyme activity and protein stability of OsDREB2B (Extended Data Fig. 14). Taken together, these data suggested that both SNP variations affect the activity of the OsSRO1c-OsDREB2B complex and play a role for modulating the transcriptional activity of OsDREB2B.

OsSRO1c^{Hap1}-OsDREB2B complex responds to cold stress via temperature-dependent LLPS *in vivo* and *in vitro*

Since the condensates formed by the OsSRO1c^{Haps}-OsDREB2B complexes showed distinct properties (size, number and FRAP recovery) in response to cold treatment (Fig. 3), we asked whether the single proteins (OsSRO1c^{Hap1} or OsDREB2B) undergo dynamic changes in response to cold or if the formation of the complex is required.

When expressed alone, we found no dynamic changes of the OsSRO1c^{Hap1} condensate signal or the OsDREB2B diffuse signal upon 2 h of cold treatment, indicating that OsSRO1c or OsDREB2B proteins alone do not respond to temperature changes (Fig. 5a,b). Next, we co-transformed mCherry- OsSRO1c^{Hap1} and GFP-OsDREB2B in tobacco leaves and observed large condensate in the nucleus under room temperature conditions, but the condensate transitioned into many smaller granule-like structures upon cold treatment (Fig. 5a,b), consistent with BiFC results (Fig. 3a). Furthermore, we examined the LLPS behavior of OsSRO1c^{Hap1}, OsDREB2B and OsSRO1c^{Hap1}-OsDREB2B complex in mammalian cells under both normal and cold stress conditions. We found that OsSRO1c^{Hap1} alone showed granule-like structures and OsDREB2B alone was uniformly distributed under both normal and cold stress conditions, while the OsSRO1c^{Hap1}-OsDREB2B complex showed homogeneous diffuse distribution under normal conditions and only formed puncta after cold stress, consistent with the tobacco system (Extended Data Fig. 15). Taken together, these results suggest that the OsSRO1c^{Hap1}-OsDREB2B complex, rather than the individual members, responds to temperature changes via the recruitment of OsDREB2B to liquid droplets upon cold treatment in mammalian and tobacco heterologous *in vivo* systems.

Next, we wondered whether the OsSRO1c^{Hap1}-OsDREB2B complex could respond to temperature changes in a simplified *in vitro* system where only OsSRO1c^{Hap1} and OsDREB2B proteins are present without the potential perturbation of other factors in the complex *in vivo* system. To this end, we purified GFP- OsSRO1c^{Hap1} and mCherry-OsDREB2B proteins and found that they co-condense into droplets when mixed *in vitro* (Fig. 5c). When photobleached, the fluorescence signal from mCherry-OsDREB2B in the co-condensed droplets could rapidly recover (Fig. 5d,e). Next, we tested whether the OsSRO1c^{Hap1}-OsDREB2B complex could directly respond to temperature changes *in vitro* by measuring the turbidity changes (an assay to quantify liquid droplet formation in bulk solution) of the protein solution when switch from room temperature to cold. After cold treatment (4℃ for 2 h), we found that the absorbance values (600

nm wavelength) of OsSRO1c^{Hap1} and OsSRO1c^{Hap1}-OsDREB2B complex were significantly increased, whereas no significant changes were observed for GFP and GFP-OsDREB2B (Fig. 5f), suggesting that both OsSRO1c^{Hap1} and OsSRO1c^{Hap1}-OsDREB2B complex have temperature dependent response *in vitro*, consistent with the *in vivo* data. In addition, we examined the turbidity of LLPS-deficient OsSRO1c^{Hap1} variants (IDR, ΔIDR, and 12RmA) in complex with OsDREB2B under both normal and cold stress conditions *in vitro*. The results showed that the protein turbidity of OsSRO1c^{Hap1} (full length)-OsDREB2B complex changed significantly after cold stress, while the protein turbidity of OsSRO1c^{Hap1} variants in complex with OsDREB2B did not show significant changes (Extended Data Fig. 16). Together, these *in vivo and in vitro* results demonstrate that the OsSRO1c-OsDREB2B co-condensate could directly respond to temperature via dynamic changes in condensate structures (number, size and fluidity), with accompanying changes in transcriptional activity.

OsDREB2B directly promotes the expression of *OsSRO1c*

Both OsSRO1c and OsDREB2B are positive regulators of the cold stress response in rice, and we next tested the expression levels of *OsSRO1c* and *OsDREB2B* during cold stress. At the early stage of cold treatment (within 24 h), the expression of *OsDREB2B* was induced first, whereas *OsSRO1c* was barely expressed. With the extension of cold stress treatment (more than 48 h), *OsSRO1c* transcripts started to accumulate and were significantly higher than that of *OsDREB2B* (Fig. 6a). OsDREB2B belongs to the DREB-type transcription factor family which binds the DRE elements (A/GCCGAC) (Matsukura *et al.*, 2010). Through DNA sequence analysis we found that there are multiple DRE elements in the promoter regions of *OsSRO1c* (Fig. 6b). Thus, we speculated that OsDREB2B might directly regulate the expression of *OsSRO1c* during the process of cold treatment. We therefore examined whether OsDREB2B can bind to the promotor region of *OsSRO1c*. Using electrophoretic mobility shift assays (EMSAs) we found that OsDREB2B could bind these DRE-containing regions *in vitro* (Fig. 6b).

In addition, chromatin immunoprecipitation followed by quantitative polymerase chain reaction (ChIP-qPCR) assays confirmed that OsDREB2B can bind the DRE regions of the *OsSRO1c* promoter *in vivo* and cold stress treatment increased the binding capacity of OsDREB2B to these regions (Fig. 6c). We also performed transient expression assays in rice protoplasts using *OsDREB2B* as effector and the firefly luciferase (*LUC*) gene driven by the promoters of *OsSRO1c* as reporter. This experiment showed that *OsDREB2B* promoted LUC activity by approximately 10 and 13-fold compared with the control under room temperature and cold stress, respectively (Fig. 6d). Moreover, we analyzed the expression levels of *OsSRO1c* in *OsDREB2B* transgenic plants (knockout and OE lines). *OsSRO1c* expression showed either no significant difference or slight decrease in *osdreb2b* mutant lines compared with the WT under both normal and cold stress conditions, respectively (Extended Data Fig. 17). In contrast, *OsSRO1c* was significantly induced in *OsDREB2B*-OE lines under normal (approximately 4-fold) and cold stress (>80 fold) (Extended Data Fig. 17). To further elucidate the genetic relationship between *OsSRO1c* and *OsDREB2B*, we generated the *ossro1c osdreb2b* (*1c2b*) double mutant, which showed similar cold sensitive phenotype as the *osdreb2b* (*2b*-CR) single mutant (Fig. 6e). However, the *1c2b* double mutant exhibited slightly lower survival rate than the *osdreb2b* single mutant after cold stress (Fig. 6f). This is likely because *OsSRO1c* is also involved in other important biological processes apart from cold stress tolerance, such as stomatal closure and hydrogen peroxide regulation as we have reported previously (You *et al.*, 2013; You *et al.*, 2014). Together, these results suggest that *OsSRO1c* is a direct downstream target gene of OsDREB2B.

The OsSRO1c-OsDREB2B complex regulates key cold tolerance gene *COLD1*

As the OsSRO1c^{Hap1}-OsDREB2B complex is important for cold tolerance, we further compared the genome-wide expression profiles of the *1c*-CR, *2b*-CR and the WT ZH11 under cold stress, aiming to find direct cold response genes that are regulated by the

OsSRO1c^{Hap1}-OsDREB2B complex. There were 4286 differentially expressed genes (DEGs) that were down regulated in both *1c*-CR and *2b*-CR under cold stress (Fig. 7a, Supplementary Table 2 and Supplementary Table 3). Gene ontology (GO) analysis of the co-downregulated genes revealed that these genes were enriched in "nuclear protein-containing complex", "transcription regulator complex" and "sequence-specific DNA binding" (Extended Data Fig. 18a), indicating the OsSRO1c^{Hap1}-OsDREB2B complex mainly functions in the transcriptional regulation of cold response. Among the co-downregulated genes, some are well-known to be involved in cold response, such as *COLD1* (Ma *et al.*, 2015), *OsMYB3R-2* (Dai et al., 2007; Ma et al., 2009) and *OsNAC6* (Nakashima et al., 2007; Hu et al., 2008). We confirmed the expression levels of these genes using qRT-PCR and the results confirmed that these genes were downregulated in the *1c*-CR and *2b*-CR mutant lines compared to WT ZH11 under cold stress (Fig. 7b and Extended Data Fig. 18b), consistent with the RNA-seq results. Next, promoter sequence analysis showed that there were two DRE elements in the promoter region of *COLD1* (Fig. 7c), thus, we speculated that *COLD1* might be a direct target of the OsSRO1c^{Hap1}-OsDREB2B complex. EMSA assays showed that OsDREB2B could specifically bind these *cis*-elements (Fig. 7c). Interestingly, when OsSRO1c^{Hap1} and OsDREB2B were co-incubated with the DNA probes, we observed a supershift band (red arrow, Fig. 7d) compared with the OsDREB2B alone (blue arrow, Fig. 7d), indicating that OsSRO1c^{Hap1}-OsDREB2B complex could bind to those probes *in vitro* (Fig. 7d). We further performed ChIP-qPCR assays in rice protoplasts and found that promoter fragments of *COLD1* were significantly enriched by OsDREB2B alone (under cold stress) and OsSRO1c^{Hap1}-OsDREB2B complex (in both normal and cold stress conditions) but not GFP (control) or OsSRO1c^{Hap1} alone (Fig. 7e), indicating that OsSRO1c^{Hap1}-OsDREB2B complex could bind to *COLD1* promotor *in vivo*. In addition, we examined the binding of the *COLD1* promoter by the OsSRO1c variants-OsDREB2B complexes, and found that natural variants of OsSRO1c, caused by SNP4361 and SNP5727, and their combination (Hap2), no longer promotes the binding

of OsDREB2B to the *COLD1* promoter (Extended Data Fig. 19). We also conducted dual luciferase activity experiments in rice protoplasts to examine the transcriptional regulation of the OsSRO1c^{Hap1}-OsDREB2B complex on *COLD1*. We found that OsDREB2B alone could only weakly promote the transcription of *COLD1*, whereas the OsSRO1c^{Hap1}-OsDREB2B complex could significantly promote the transcription of *COLD1* under both room temperature and cold stress (Fig. 7f). Furthermore, we examined the Ca^{2+} signaling in *ossro1c osdreb2b* single and double mutants after cold stress. Upon cold stimulation, the degree of influx of extracellular Ca^{2+} in *ossro1c* mutant (*1c*-CR), *osdreb2b* mutant (*2b*-CR) and *ossro1c osdreb2b double mutant* (*1c2b*-2) were all weaker than that in wild-type ZH11 roots (Extended Data Fig. 20). This result is consistent with that of *COLD1* mutant (*cold1-1*) (Ma *et al.*, 2015), indicating that OsSRO1c^{Hap1}-OsDREB2B complex can positively regulate *COLD1* and Ca^{2+} influx under cold stress. Taken together, these results suggest that *COLD1* is a direct target gene of the OsSRO1c^{Hap1}-OsDREB2B complex.

Discussion

Rice is a cold-sensitive crop whose productivity faces great challenges in the era of global climate change when cold stress conditions are more frequent. Identifying superior alleles from rice germplasms that confer cold tolerance is a major approach toward breeding cold tolerant rice varieties. In this study, we demonstrate that *OsSRO1c* is a positive regulator in rice cold tolerance. We further show that while variants, OsSRO1c^{Hap1} and OsSRO1c^{Hap2}, co-condense with OsDREB2, OsSRO1c^{Hap1}-OsDREB2 condensates most strongly activate key cold responsive genes, including *COLD1* (Ma *et al.*, 2015). Importantly, introgression of the strong OsSRO1c^{Hap1} allele into a cold stress susceptible conventional *indica* variety, Guichao#2, could significantly increase both its survival rate in the seedling stage and seed setting rate in the booting stage under cold stress, demonstrating that OsSRO1c^{Hap1} possesses promising potential in breeding cold tolerant rice.

It has been shown that the SRO proteins are involved in a variety of abiotic stress responses by interacting with transcription factors and regulating their transcriptional activities. For example, the maize SRO protein, ZmSRO1e, represses the transcriptional activity of the MYB-bHLH-WD40 transcriptional activation complex (Qin et al., 2021) and the chrysanthemum SRO protein, CmRCD1, represses the transcriptional activity of CmBBX8 and interferes with its binding to the *CmFTL1* promoter (Wang et al., 2021). However, the underlying molecular mechanisms of SRO family proteins are still largely unclear. In this study, we found that OsSRO1c, a member of the rice SRO protein family, could positively regulate the transcriptional activity of OsDREB2B by recruiting OsDREB2B into condensates (Fig. 3), with the OsSRO1c^{Hap1} allele exhibiting the strongest transcriptional effect and exhibiting the most dynamic condensates based on in vivo and in vitro FRAP assays. Previously, several studies have reported that SRO proteins have unusual subcellular localization. For example, AtSRO5-GFP fusion protein has been reported to locate to several dot-like structures

485 in the nucleus (Jaspers *et al.*, 2010), while expressing RCD1-Venus in *rcd1* mutant
486 reveals the localization of distinct nuclear bodies (NBs) (Vainonen et al., 2023).
487 Additionally, subcellular localization of ZmSRO1d in maize protoplasts performs
488 granule-like structures in the nucleus (Gao *et al.*, 2022) and BiFC assays between the
489 bread wheat SRO protein TaSRO1 and the NAC transcription factor TaSIP1 yielded a
490 punctate pattern in the cytoplasm (Wang *et al.*, 2022). However, the function of these
491 SRO protein puncta remained a mystery. In this work, we found that OsSRO1c exhibits
492 a granular structure in rice root-tip cells, rice protoplasts and in the heterologous system
493 of tobacco leaves. We further show that these granular structures are protein
494 condensates formed via LLPS (Fig. 4). Furthermore, we demonstrate that OsSRO1c
495 with LLPS ability, and most notably the OsSRO1c^{Hap1} variant, can promote the
496 transcriptional activity of OsDREB2B. Conversely, OsSRO1c with reduced or
497 abolished LLPS ability has no effect on the transcriptional activity of OsDREB2B (Fig.
498 4). Thus, our work suggests that OsSRO1c, and in particular the OsSRO1c^{Hap1} allele,
499 acts as a transcriptional co-activator of OsDREB2B via protein co-condensation,
500 resulting in an increase in OsDREB2B transcriptional activity. Transcription factors
501 and/or co-activators showing altered transcriptional activity via forming protein
502 condensation has been reported in animal systems (Boija et al., 2018; Zamudio et al.,
503 2019), but few known cases are available in plant system (Wang et al., 2023).
504 Protein LLPS has been emerging as an important principle for the understanding of
505 diverse biological processes in living cells and was proposed to be a key mechanism
506 for environment and stress sensing (Noguchi and Kodama, 2022; Jung *et al.*, 2023;
507 Kerbler and Philip, 2023). For example, the Arabidopsis circadian clock protein ELF3
508 senses elevated ambient temperature via temperature-dependent LLPS, while cold
509 exposure rapidly promotes the formation of FRI-containing nuclear condensates (Jung
510 *et al.*, 2020; Zhu *et al.*, 2021). In this study, we found that the OsSRO1c-OsDREB2B
511 complex can respond to cold stress via cold induced LLPS. Intriguingly, OsSRO1c-
512 OsDREB2B complex exhibited the formation of a single large condensate under normal

conditions, which rapidly transformed into multiple small droplets upon cold treatment (Fig. 3 and Fig. 5). Multiple small punctate structures after cold stress had better mobility than the large condensate under normal conditions and enhanced the transcriptional activity of OsDREB2B, most strikingly for the OsSRO1c^{Hap1}-OsDREB2 complex. Thus, OsSRO1c-OsDREB2B condensate is not only directly responsive to temperature changes, but also render a direct output effect—the elevation of OsDREB2B activity and the subsequent cold stress responses. Interestingly, LLPS behavior of OsSRO1c alone also changed after cold stress *in vivo* (Fig. 5a,b) and *in vitro* (Fig. 5e), although not as significantly as the OsSRO1c-OsDREB2B complex. It would be interesting in the future to investigate more rigorously whether OsSRO1c or the complex is able to alter its protein conformation and change its LLPS behavior in response to different temperature changes, and if there is any, what is the underlying mechanism, in order to address the cold sensor function of OsSRO1c and the complex. Furthermore, whether SRO proteins with the PARP domain can perform the function of poly(ADP-ribose) polymerase has not been definitively determined. So far, only wheat member TaSRO1 has been reported to be capable of poly(ADP-ribosyl)ation (PARylation) (Liu *et al.*, 2014). Subsequently, SRO2 (Kong *et al.*, 2021) and ZmSRO1d (Gao *et al.*, 2022) have been reported to perform noncanonical mono(ADP-ribosyl)ation. Surprisingly, although RCD1 was previously shown to be inactive (Jaspers *et al.*, 2010), recently, it was found that RCD1 could directly bind PAR *in vitro* and such binding resulted in the subnuclear localization of RCD1 to nuclear bodies (NBs) (Vainonen *et al.*, 2023). These findings provide a new direction as to further study whether the low levels of OsSRO1c poly/mono(ADP-ribosyl)ation activity we detected are functionally important and the putative role of PARylation or MARylation post-translational modification processes in OsSRO1c function.

In summary, this study has revealed the role of OsSRO1c and its interacting transcription factor OsDREB2B in the cold stress response in rice. OsSRO1c possesses intrinsic LLPS properties and co-condensates with OsDREB2B in the nucleus. The

OsSRO1c-OsDREB2B droplet can directly sense cold stress by transitioning into smaller droplets with increased protein mobility, particularly the OsSRO1c^{Hap1} variant (Fig. 7g). The droplet formed by the OsSRO1c^{Hap1}-OsDREB2B complex derived from the strong haplotype is more dynamic than that of OsSRO1c^{Hap2}-OsDREB2B complex derived from the weak haplotype, and able to better promote the transcriptional activity of OsDREB2B, activating the key cold response gene *COLD1*, resulting in the cold resistance phenotype of the strong allele. Thus, our work reveals a novel mechanism of cold stress sensing by the OsSRO1c-OsDREB2B complex through protein phase transition and provides evidence that OsSRO1c^{Hap1}is a highly valuable gene for breeding cold tolerance rice varieties.

Materials and methods

Association analysis of candidate genes

The GWAS data were from our previous work (Lv *et al.*, 2016). The position of SNPs in *OsSRO1c* were based on data from the MSU Rice Genome Annotation Project (http://rice.plantbiology.msu.edu). The Manhattan and LD plots were drawn using the R package. The haplotype analysis and subpopulation data were obtained from the database RiceVarMap (http://ricevarmap.ncpgr.cn/). Boxplots were drawn using the R package ggplot2.

Plant materials

To construct knockout plants by CRISPR/Cas9 technology, the guide RNA sequences of *OsSRO1c* or *OsDREB2B* were obtained from the CRISPR-P 2.0 database (http://crispr.hzau.edu.cn/CRISPR2/) and cloned into the *TKC* (He et al., 2018) or *PRGEB* (Xie et al., 2015) vector for *1c*-CR or *2b*-CR, respectively. To construct overexpression plants, the full-length coding sequences (CDS) of *OsSRO1c* and *OsDREB2B* were cloned into the pCAMBIA1301U vector (for *OsSRO1c*-OE and *OsDREB2B*-OE) driven by the maize *Ubiquitin* promoter. The plasmids were introduced into the *japonica* rice (*O. sativa*) variety Zhonghua11 (ZH11) by *Agrobacterium tumefaciens* mediated transformation. The CRISPR target and primer sequences for vectors are listed in Supplementary Table 4.

To construct complementary plants, the upstream 2 kb region of *OsSRO1c* start codon and different haplotypes OsSRO1c CDS sequence were cloned into the pCAMBIA2301U vector (for complementary plants Com^{Hap1} and Com^{Hap2}) and the plasmids were introduced into the *OsSRO1c* CRISPR materials by *Agrobacterium tumefaciens* mediated transformation. Primer sequences for vectors are listed in Supplementary Table 4.

To develop the introgression line, an elite indica variety Guichao#2, with the weak haplotype *OsSRO1c*^{Hap2} was used as the recipient parent. The Vietnam cultivar OM1723 with the strong haplotype *OsSRO1c*^{Hap1} was used as the donor parent. OM1723 was crossed with Guichao#2 to obtain F_1 seeds, backcrossed with Guichao#2 for four generations to get BC_4F_1 and self-crossed for two generations to get BC_4F_3. During the backcross, *OsSRO1c*^{Hap1} was selected by using the marker R0621 and R0689 **(**Supplementary Table 4**)**. The introgression line carried an OM1723 genomic segment (approximately 650 kb) containing *OsSRO1c*^{Hap1}, and the BC_4F_4 generation was used in this study.

Cold stress treatments

For the seedling-stage cold stress treatment, after 7 d of germination, transgenic plants and the wild-type ZH11 were planted in pots with soil and grown under normal conditions during the natural rice-growing seasons in the experimental fields of Huazhong Agricultural University, Wuhan, China. At the four-leaf stage, half of the seedlings were transferred to a 4±1°C chamber for cold stress, and the other half remained in the normal growth conditions as control. After 3-5 d, the cold treated plants were transferred back to normal growth conditions for recovery.

For the booting-stage cold stress treatment, the Guichao#2 and NIL- *OsSRO1c*^{Hap1} plants were planted one plant per pots and grown under normal conditions during the natural rice-growing seasons in the experimental fields of Huazhong Agricultural University, Wuhan, China. At the booting-stage, the plants were transferred to a 16± 1°C chamber for 7 d and then transferred back to normal growth conditions until maturity. The spikes numbers were taken to calculate the seed setting rates.

Relative electrolyte leakage measurement

The relative electrolyte leakage measurement was performed as previously described (Lv *et al.*, 2016) with minor modifications. Three fully expanded leaves from three

plants were cut into segments of similar sizes and immersed in 3.5 mL of double distilled water in a 10 mL test tube for 24 h continual shaking at a speed of 100 rpm at room temperature. The initial conductivity (E1) was measured with a conductivity meter (Model DDSIIA, Shanghai Leici Instrument Inc., Shanghai, China). Then, the test tubes were placed in boiling water for 15 min and cooled naturally to room temperature, and the conductivity (E2) was determined again. The relative electrolyte leakage was calculated as the ratio of E1 to E2.

Pull-down assay

The CDS of *OsSRO1c* was cloned into plasmid pMALc2x as a maltose-binding protein (MBP)-fusion protein (OsSRO1c^{Haps}-MBP); *OsDREB2B* was subcloned into polyhistidine (His) containing plasmid pET32a to generate fusion proteins of OsDREB2B-His. The two fusion proteins were expressed in *Escherichia coli* BL21 (TransGen, CD601-02) and purified *in vitro*. For pull-down assays, 1 μg of OsDREB2B-His prey proteins were incubated with immobilized MBP (1 μg) or OsSRO1c^{Haps}-MBP (1 μg) bait proteins at 4°C for 1 h. Then 30 μL of Ni-NTA agarose (Qiagen, 133223438) was added into the mixture and continually incubated at 4°C for 1 h. After extensive washing and boiling, the pull-down proteins were analyzed by western blot using anti-MBP antibody (Abclonal, AE016) and anti-His (Abclonal, AE003) antibody.

Rice protoplast isolation and transformation

Rice protoplasts were used to perform BiFC, Co-IP, subcellular localization and trans-activation assays. The rice protoplast isolation and transformation was performed as described previously (Xie and Yang, 2013). Briefly, the shoots of two-week stage rice seedlings were cut into 1 mm segments and infiltrated in digestion solution including 10 mM MES (pH5.7), 0.6 M mannitol, 1 mM $CaCl_2$, 0.1% BSA, 0.75% Cellulase R10 (Yakult Pharmaceutical), and 0.75% Macerozyme R10 for 30 minutes in a vacuumized

chamber. The rice protoplasts were continued to shake for 4 h under dark conditions on a 60 rpm shaker. The following collection and incubation were performed in W5 solution (2 mM MES, pH5.7, 154 mM NaCl, 5 mM KCl, and 125 mM $CaCl_2$) at room temperature, then the protoplasts were filtered through a sieve mesh and resuspended in 4 mM MES, 0.6 mannitol, and 15 mM $MgCl_2$ after centrifugation at 200 g for 10 min. Each transformation contained 10 μL of different plasmids, 100 μL of protoplasts, and 110 μL of polyethylene glycol-$CaCl_2$ solution (0.6 M mannitol, 100 mM $CaCl_2$, and 40% polyethylene glycol 4000). After incubation at room temperature for 10 min, 440 μL of W5 solution was added to stop the process. After centrifugation at 200 g for 10 min, the transformed protoplasts were cultured in 800 μL of WI buffer containing 4 mM MES, pH5.7, 0.6 M mannitol, and 4 mM KCl at room temperature for overnight.

Co-immunoprecipitation (Co-IP)

OsSRO1c^{Haps} and OsDREB2B were fused with 3×HA and 3×Flag tag, respectively. These constructs were co-transformed into rice protoplasts and the HA empty vector PM999-HA was used as the negative control. After an incubation period in the dark for 16 h, the protoplasts were collected and resuspended in 600 μL of co-IP buffer (50 mM Tris-HCl (pH8.0), 150 mM KCl, 1 mM EDTA, 0.5% Triton X-100, 1 mM DTT, 1 mM PMSF, and 1× Protease Inhibitor Cocktail (Roche)). The protoplast proteins were collected from the supernatant after centrifugation at 12,000 rpm for 15 min at 4°C, and 10% of the supernatant was used as the input sample. A total of 40 μL of HA-Trp beads (Chromotek) and the supernatant from the two transformations were mixed and incubated with gentle rolling at 4°C for 4 h. Then, the beads were resuspended in 50 μL of 1× Laemmli buffer after washing with co-IP buffer for five times. The immunocomplexes were analyzed by western blot using Anti-Flag (Sigma, F1804, USA) and Anti-HA (Abclonal, AE008) antibodies.

Luciferase Complementation Assay (LCA)

To perform LCA assay in tobacco leaves, the CDS of *OsSRO1c*^{Haps} were cloned into the NLuc vector and the *OsDREB2B* CDS was cloned into the CLuc vector (Zhou et al., 2018). The constructs were transformed into *Agrobacterium tumefaciens* strain GV3101 (WEIDI, AC1001) and cultured overnight in 3 mL of LB medium containing 50 μg mL^{-1} kanamycin and 50 μg mL^{-1} rifampin at 28°C. The bacteria were collected, mixed, and infiltrated into young leaves of *N. benthamiana* plants, and the infiltrated leaves were analyzed for LUC activity using chemiluminescence imaging (Tanon 5200) 36 h after infiltration. The leaf was sprayed with 1 mM D-luciferin (YEASEN, 40902ES03) and then imaged 10 min later.

Bimolecular fluorescence complementation (BiFC)

To perform BiFC assay in rice protoplasts, the CDS of *OsSRO1c*^{Haps} were cloned into the pVYNE vector and the *OsDREB2B* CDS was cloned into the pVYCE vector (Waadt et al., 2008). Plasmids were transformed into rice protoplasts by polyethylene glycol-mediated transformation. GFP fluorescence was visualized with a confocal scanning microscope (Carl Zeiss, LSM980, Germany) after incubation in the dark for 16 h at room temperature.

To perform BiFC assay in tobacco leaves, the CDS of *OsSRO1c* was cloned into the vector pEarleygate201-YN, whereas *OsDREB2B* was cloned into the vector pEarleygate202-YC. The constructs were transformed into *Agrobacterium tumefaciens* and bacteria were infiltrated into tobacco leaves with the same methods mentioned above. GFP fluorescence was visualized with a confocal scanning microscope (Carl Zeiss, LSM980, Germany) after infiltration of 36 h. The relative area of condensate was quantified using ZEN software whereas the number and the average area of granules were quantified using ImageJ.

Fluorescence recovery after photobleaching (FRAP) assay

The FRAP analysis was performed on a Zeiss LSM980. GFP fluorescence was detected using a ×40 objective. The FRAP model of Zeiss LSM980 was as follows: for the pre-bleach, one granule was first recorded with 2 iterations to determine the stability of the signal itself, then the granule was bleached with 20 iterations using a laser intensity of 95% at 488 nm. After bleaching, images were recorded with 30 iterations. The time per-iteration was 2 s. The recovery curves were generated with ZEN software.

Subcellular localization

To perform subcellular localization in rice protoplasts, the CDSs of *OsSRO1c* and *OsDREB2B* were cloned into a plant transient expression vector (PM999-GFP) with a C-terminal GFP fusion. Ghd7-mCherry was used as nucleus marker (Xue et al., 2008). Plasmids were transformed into rice protoplasts and cultured in the dark for 16 h at room temperature.

To perform subcellular localization in tobacco leaves, the CDSs of *OsSRO1c* and *OsDREB2B* were cloned into the vector HGF with a N-terminal GFP fusion. The constructs were transformed into *Agrobacterium tumefaciens* and bacteria were infiltrated into tobacco leaves. Transformed protoplasts and infiltrated tobacco leaves were observed with a confocal microscope (Carl Zeiss, LSM980, Germany).

In vitro droplet assay

His_6-GFP tagged OsSRO1c and His_6-mCherry tagged OsDREB2B protein were purified *in vitro* using Ni-NTA agarose (Qiagen, 133223438). Concentration gradient dilution was performed in a buffer containing 20 mM Tris-HCl (pH8.0), 100 mM NaCl and 5% PEG6000 (Sangon, A610432-0500). Droplets were observed using a Zeiss LSM980 microscope equipped with a ×40 objective.

In vitro turbidity measurement

Turbidity of protein samples was measured based on the optical absorption at 600 nm (Zhu et al., 2022). Equal molar concentration (5 μM) of the protein samples (OsSRO1c and OsDREB2B) were mixed in the same buffer as the *in vitro* droplet assays. The optical absorption was recorded on a TECAN-Spark Multifunctional Enzyme Labeler using a flat bottom and low volume 384-well plates (Corning). Protein samples were incubated for 2 h at 4°C and assayed for absorbance values before and after cold stress treatment.

Total RNA isolation and RT-qPCR analysis

Total RNA was extracted using TransZol (TransGen Biotech, ET101-01) and reverse transcribed using EasyScript One-Step gDNA Removal and cDNA Synthesis SuperMix kit (TransGen Biotech, AE311-03) according to the manufacturer's instructions. Quantitative PCR reactions were performed in 384-well blocks with the QuantStudio 6 Flex System (Thermo Fisher Scientific) using 2×SYBR qPCR Mix (Cookgen, KKR012) in a final volume of 10 μL. *ACTIN2* was used as an internal control. The primers used for RT-qPCR are listed in Supplementary Table 4.

Electrophoretic mobility shift assays (EMSA)

The CDS of *OsDREB2B* was inserted into the pET32a expression vector and expressed in *E.coli* BL21 (TransGen, CD601-02). The His_6 tagged fusion protein was purified with Ni-NTA agarose (Qiagen, 133223438). The probes of *OsSRO1c* and *COLD1* promoters were synthesized by Beijing TsingKe with 5' FAM labeled. The double-stranded oligonucleotides were generated by mixing with an equal amount of the complementary single stranded oligonucleotides for 2 min at 95°C and cooled down to 25°C. EMSA was performed using the LightShift Chemiluminescent EMSA Kit (Thermo Scientific, 20148). The purified His-fused OsDREB2B and probes were incubated with the binding buffer (1 mg of poly(dI-dC), 10 mM Tris-HCl (pH7.5), 50

mM KCl, 1 mM DTT, 2.5% glycerol, and 5 mM $MgCl_2$) at room temperature for 30 min. Then the samples were run on a 6.5% PAGE gel with 0.5× Tris-borate-EDTA buffer for 1 h at 4°C. The fluorescence signal was captured by FLA-5100 (Fuji). Probe sequences are listed in Supplementary Table 4.

ChIP-qPCR

To perform ChIP assays, 30 μg OsDREB2B-GFP and GFP empty vectors were transformed into 1 mL rice protoplasts, respectively. After cultured overnight, rice protoplasts were collected and immediately fixed with 1% formaldehyde for chromatin crosslinking. Chromatin was isolated after cell lysis, nucleus lysis and ultrasonic crushing, then immunoprecipitated using Anti-GFP Nanobody Magarose Beads (AlpaLifeBio, KTSM1334) in IP buffer containing 20 mM Tris-HCl, 1 mM EDTA, 0.1% NP-40, 10% glycerol, pH7.5, and freshly added proteinase inhibitor at 4℃ for overnight. The immunoprecipitated DNA were eluted in buffer containing 1% SDS and 0.1M $NaHCO_3$, and isolated in sodium acetate ethanol solution.

For quantifications using real-time PCR (ChIP-qPCR), the relative fold change was calculated according to the $2^{-\Delta Ct}$, where ΔCt =Ct (OsDREB2B-GFP)-Ct (GFP), where Ct is the mean threshold cycle of the corresponding PCR reaction. Primer sequences for ChIP-qPCR are listed in Supplementary Table 4.

Trans-activation activity assay in rice protoplasts

To examine $OsSRO1c^{Haps}$ influence on the transcriptional activity of OsDREB2B, the CDS of *OsSRO1c*^{Haps} were cloned into the NONE vector as effectors. The CDS of *OsDREB2B* was cloned into the GAL4BD vector which containing the GAL4 DNA binding domain and driven by the *CaMV35S* promoter. The *firefly luciferase* (F-LUC) gene located downstream of the *CaMV35S* enhancer and five copies of the GAL4 binding element was used as reporter, while the *renilla luciferase* (R-LUC) gene driven

by the Arabidopsis *Ubiquitin3* promoter was used as internal control. The plasmids were co-transformed into rice protoplasts in a ratio of 6:6:6:1.

To examine the regulation of OsDREB2B on *OsSRO1c*, the CDS of *OsDREB2B* was cloned into the NONE vector as effector, while the promoter of *OsSRO1c* was amplified and cloned into the 190LUC vector containing the firefly luciferase gene as reporter. The R-LUC vector was used as internal control. The plasmids were co-transformed into rice protoplasts in a ratio of 6:6:1.

Rice protoplasts were incubated for 16 h in the dark at room temperature. After incubation, half of the transformed protoplast populations was cold treated at 4°C in the dark for 1 h, the other half remained in room temperature as control. Finally, protoplasts were collected by centrifugation at 200 g for 10 min and immediately utilized for luciferase assays. Luciferase activity was quantified using the Dual Luciferase Reporter Assay System (Promega) according to the manufacturer's instructions. Six independent transformations for each sample were performed, and the relative luciferase activity was calculated as the ratio of F-LUC to R-LUC.

RNA-seq analysis

RNA-seq analysis was performed using the mutants *1c*-CR, *2b*-CR and wild type ZH11. The four-leaf stage seedlings after 4°C cold stress for 2 d were harvested for total RNA extraction as described above. The RNA-seq data were sequenced at the Beijing Novogene company and analyzed on the servers of National Key Laboratory of Crop Genetic Improvement. Briefly, the raw data was filtered and quality controlled using fastp software (Chen et al., 2018). The clean data was mapped to the reference genome (MSU 7.0 version) using software HISAT2 (Pertea et al., 2016). The gene raw count was calculated using software StringTie (Pertea et al., 2015). The DEGs were analyzed by R package DESeq2 and identified with fold change ≥ 1.5 and $P < 0.05$. The R package clusterProfiler (Yu et al., 2012) was used for gene ontology (GO) analysis.

Representative genes were confirmed by RT-qPCR. The primers are listed in Supplementary Table 4.

Statistical analysis

All data analyses were performed using GraphPad Prism 8.2.1 Software. Unpaired two-tailed Student's *t*-test was used for significant difference analysis between two samples. One-way ANOVA analyses followed with Tukey's test ($P < 0.05$) were used for pairwise multiple comparisons. The imageJ software was used to analyze the area and number of puncta. The ZEN 3.0 software was used to analyze confocal images and FRAP curves.

PARP activity assay *in vitro*

The CDSs of *SRO2*, *AtPARP2*, *OsSRO1c* or its variants were placed in the pET32a vector, and the different plasmids were then transformed into *Escherichia coli* BL21 (TransGen, CD601-02). The proteins were purified *in vitro* and used for the PARP enzyme activity assay. The protein bands of the target proteins were subsequently quantified based on serial dilutions of BSA as the standard, through ImageJ intensity quantification. An equal amount of purified protein was used for the PARP activity assay, which was conducted using the PARP Universal Colorimetric Assay Kit (Trevigen; 4677-096-K) following the manufacturer's protocol. PARP-HSA Enzyme The PARP-HSA Enzyme in the kit was used as positive control, and PARP Buffer in the kit was used as negative control. Reported SRO2 and AtPARP2 were also used for reference.

OsSRO1c^{Haps}-OsDREB2B complex protein levels detection

For detection of the protein levels of OsSRO1c^{Haps}-OsDREB2B complex in rice protoplasts. The CDS of *OsSRO1c* or its variants were cloned into plasmid PM999-HA vector (OsSRO1c^{Haps}-HA), and *OsDREB2B* was cloned into PM999-GFP vector (OsDREB2B-GFP). 100 μl rice protoplasts were co-transformed by 3 μg of

OsSRO1c^{Haps}-HA plasmid and 3 μg of OsDREB2B-GFP plasmid, and cultured overnight at room temperature in dark. Total protein was extracted and used for Western Blot.

For detection of the protein levels of OsSRO1c^{Haps}-OsDREB2B complex in tobacco leaves. The same vectors were transformed into *Agrobacterium tumefaciens* strain GV3101 (WEIDI, AC1001) and cultured overnight in 3 mL of LB medium containing 50 μg mL^{-1} kanamycin and 50 μg mL^{-1} rifampin at 28°C. The bacteria were collected, re-suspended with buffer (10 mM MES; 200 μM AS; 10 mM $MgCl_2$) and adjusted to a consistent concentration by OD_{600}. Equal amounts of OsSRO1c^{Haps}-HA and OsDREB2B-GFP bacteria were mixed, injected into tobacco leaves, and cultured for 36 h. Total protein was extracted from 0.1 g leaves and used for Western Blot.

The protein levels of OsDREB2B-GFP and OsSRO1c^{Haps}-HA were detected by GFP and HA antibodies (ABclonal, AE078, AE008), respectively, and the equal sample loading was evaluated by plant-specific actin antibody (ABclonal, AC009).

Measurement of Ca^{2+} Flux with the NMT

The roots of 2-week-old seedlings were used to detect Ca^{2+} using flux Non-invasive Micro-test Technique (NMT-YG-100, YoungerUSA LLC, Amherst, MA01002, USA) and imFluxes software. Pre-pulled and silanized microsensor (⌀4.5 ± 0.5 μm, XY- STZ-Ca-T) were filled with a backfilling solution (100 mM $CaCl_2$) to a length of nearly 1.0 cm and then 50 μm columns of selective liquid ion-exchange cocktails (LIXs, Ca^{2+}: XY-SJ-Ca. Younger, USA) were filled from the tip. Prior to the flux measurement, the roots were incubated in the measuring solution (1.0 mM KCl, 0.2 mM $CaCl_2$, and 0.2 mM MES, pH 5.8) for 5 min. For cold stress, the roots were incubated in measuring solution at 0℃. The microsensor was calibrated with 0.1, 0.5 or 1 mM $CaCl_2$ in calibration liquid (1.0 mM KCl, 0.2 mM $CaCl_2$, and 0.2 mM MES, pH 5.8). Ion fluxes were measured in the zone about 30 μm from the tip.

Mammalian cell transformation

The CDSs of *OsSRO1c* and *OsDREB2B* were cloned in the PML28-EGFP, PML28-yn and PML28-yc vector, and the different plasmids were then transformed into *Escherichia coli* DH5α (Tsingke, TSC-C14). The plasmids were extracted with EndoFree Plasmid Midi Kit (CWBIO, CW2105S) to remove endotoxin. A total of 2 mg plasmid transformed HEK293T cells (Invitrogen, A14527). After the transfection mixture was added to the cell culture, the culture was gently rotated at room temperature for 40 min and then cultured for 36 to 48 h. The cultured cells were treated at 4℃ for 2 h and then observed with a confocal microscope (Carl Zeiss, LSM980, Germany).

Population genetic analysis

The single-nucleotide polymorphism data of the *OsSRO1c* from 527 rice varieties were collected from the RicevarMap database (http://ricevarmap.ncpgr.cn/). The phylogenetic tree was visualized and annotated using 'iTOL' (https://itol.embl.de/login.cgi). The population differentiation (F_{ST}) and nucleotide diversity statistics (π) of *OsSRO1c* was computed using software vcftools (Danecek et al., 2011).

Data availability

RNA-seq data generated in this study have been deposited in the GEO database under accession no. GSE247749.

Acknowledgments

This work was supported by grants from the National Key Research and Development Program of China (2022YFF1001604), distinguished young scholar grant from the Department of Science and Technology of Hubei Province (2023AFA095), and Huazhong Agricultural University Independent Science and Technology Innovation Fund (304/510322064). The computations in this paper were run on the bioinformatics

computing platform of the National Key Laboratory of Crop Genetic Improvement, Huazhong Agricultural University.

Author contributions

D.H., X.L. and L.X. designed the study. D.H., Y.Y., Y.Lv. and J.You. performed all experiments. D.H., Y.Y., H.Xiong. and X.L. analysed the data. D.H., S.H., C.Z., X.L. and L.X. wrote and revised the article.

Competing interests

The authors declare no competing interests.

References

Boija, A., Klein, I.A., Sabari, B.R., Dall'Agnese, A., Coffey, E.L., Zamudio, A.V., Li, C.H., Shrinivas, K., Manteiga, J.C., Hannett, N.M., et al. (2018). Transcription Factors Activate Genes through the Phase-Separation Capacity of Their Activation Domains. Cell **175**:1842-1855 e1816. 10.1016/j.cell.2018.10.042.

Bugge, K., Staby, L., Kemplen, K.R., O'Shea, C., Bendsen, S.K., Jensen, M.K., Olsen, J.G., Skriver, K., and Kragelund, B.B. (2018). Structure of Radical-Induced Cell Death1 Hub Domain Reveals a Common alphaalpha-Scaffold for Disorder in Transcriptional Networks. Structure **26**:734-746 e737. 10.1016/j.str.2018.03.013.

Buttress, T., He, S., Wang, L., Zhou, S., Saalbach, G., Vickers, M., Li, G., Li, P., and Feng, X. (2022). Histone H2B.8 compacts flowering plant sperm through chromatin phase separation. Nature **611**:614-622. 10.1038/s41586-022-05386-6.

Chen, J.Q., Meng, X.P., Zhang, Y., Xia, M., and Wang, X.P. (2008). Over-expression of OsDREB genes lead to enhanced drought tolerance in rice. Biotechnol. Lett. **30**:2191-2198. 10.1007/s10529-008-9811-5.

Chen, S., Zhou, Y., Chen, Y., and Gu, J. (2018). fastp: an ultra-fast all-in-one FASTQ preprocessor. Bioinformatics **34**:i884-i890. 10.1093/bioinformatics/bty560.

Cheng, S.L.H., Wu, H.-W., Xu, H., Singh, R.M., Yao, T., Jang, I.-C., and Chua, N.-H. (2022). Nutrient status regulates MED19a phase separation for ORESARA1-dependent senescence. New Phytol. **236**:1779-1795. 10.1111/nph.18478.

Dai, X., Xu, Y., Ma, Q., Xu, W., Wang, T., Xue, Y., and Chong, K. (2007). Overexpression of an R1R2R3 MYB Gene, OsMYB3R-2, Increases Tolerance to Freezing, Drought, and Salt Stress in Transgenic Arabidopsis. Plant Physiol. **143**:1739-1751. 10.1104/pp.106.094532.

Danecek, P., Auton, A., Abecasis, G., Albers, C.A., Banks, E., DePristo, M.A., Handsaker, R.E., Lunter, G., Marth, G.T., Sherry, S.T., et al. (2011). The variant call format and VCFtools. Bioinformatics **27**:2156-2158. 10.1093/bioinformatics/btr330.

Ding, Y., and Yang, S. (2022). Surviving and thriving: How plants perceive and respond to temperature stress. Dev. Cell **57**:947-958. 10.1016/j.devcel.2022.03.010.

Gao, H., Cui, J., Liu, S., Wang, S., Lian, Y., Bai, Y., Zhu, T., Wu, H., Wang, Y., Yang, S., et al. (2022). Natural variations of ZmSRO1d modulate the trade-off between drought resistance and yield by affecting ZmRBOHC-mediated stomatal ROS production in maize. Mol Plant **15**:1558-1574. 10.1016/j.molp.2022.08.009.

Gu, S., Zhang, Z., Li, J., Sun, J., Cui, Z., Li, F., Zhuang, J., Chen, W., Su, C., Wu, L., et al. (2023). Natural variation in OsSEC13 HOMOLOG 1 modulates redox homeostasis to confer cold tolerance in rice. Plant Physiol. 10.1093/plphys/kiad420.

Hayes, S., Schachtschabel, J., Mishkind, M., Munnik, T., and Arisz, S.A. (2021). Hot topic: Thermosensing in plants. Plant Cell Environ **44**:2018-2033. 10.1111/pce.13979.

He, Y., Zhu, M., Wang, L., Wu, J., Wang, Q., Wang, R., and Zhao, Y. (2018). Programmed Self-Elimination of the CRISPR/Cas9 Construct Greatly Accelerates the Isolation of Edited and Transgene-Free Rice Plants. Mol Plant **11**:1210-1213. 10.1016/j.molp.2018.05.005.

Hu, H., You, J., Fang, Y., Zhu, X., Qi, Z., and Xiong, L. (2008). Characterization of transcription factor gene SNAC2 conferring cold and salt tolerance in rice. Plant Mol. Biol. **67**:169-181. 10.1007/s11103-008-9309-5.

Huang, X., Kurata, N., Wei, X., Wang, Z.X., Wang, A., Zhao, Q., Zhao, Y., Liu, K., Lu, H., and Li, W. (2012). A map of rice genome variation reveals the origin of cultivated rice. Nature **490**:497-501.

Hutin, S., Kumita, J.R., Strotmann, V.I., Dolata, A., Ling, W.L., Louafi, N., Popov, A., Milhiet, P.-E., Blackledge, M., Nanao, M.H., et al. (2023). Phase separation and molecular ordering of the prion-like domain of the Arabidopsis thermosensory protein EARLY FLOWERING 3. Proc Natl Acad Sci U S A **120**:e2304714120. 10.1073/pnas.2304714120.

Jaspers, P., Overmyer, K., Wrzaczek, M., Vainonen, J.P., Blomster, T., Salojarvi, J., Reddy, R.A., and Kangasjarvi, J. (2010). The RST and PARP-like domain containing SRO protein family: analysis of protein structure, function and conservation in land plants. BMC Genomics **11**:170. 10.1186/1471-2164-11-170.

Jaspers, P., Blomster, T., Brosche, M., Salojarvi, J., Ahlfors, R., Vainonen, J.P., Reddy, R.A., Immink, R., Angenent, G., Turck, F., et al. (2009). Unequally redundant RCD1 and SRO1 mediate stress and developmental responses and interact with transcription factors. Plant J. **60**:268-279. 10.1111/j.1365-313X.2009.03951.x.

Jung, J.-H., Seo, P.J., Oh, E., and Kim, J. (2023). Temperature perception by plants. Trends Plant Sci. **28**:924-940. 10.1016/j.tplants.2023.03.006.

Jung, J.H., Barbosa, A.D., Hutin, S., Kumita, J.R., Gao, M., Derwort, D., Silva, C.S., Lai, X., Pierre, E., Geng, F., et al. (2020). A prion-like domain in ELF3 functions as a thermosensor in Arabidopsis. Nature **585**:256-260. 10.1038/s41586-020-2644-7.

Kerbler, S.M., and Philip, A.W. (2023). Temperature Sensing in Plants. Annu. Rev. Plant Biol. **74**:341-366. 10.1146/annurev-arplant-102820-102235.

Kong, L., Feng, B., Yan, Y., Zhang, C., Kim, J.H., Xu, L., Rack, J.G.M., Wang, Y., Jang, J.C., Ahel, I., et al. (2021). Noncanonical mono(ADP-ribosyl)ation of zinc finger SZF proteins counteracts ubiquitination for protein homeostasis in plant immunity. Mol. Cell **81**:4591-4604 e4598. 10.1016/j.molcel.2021.09.006.

Li, C., and Fang, X. (2020). Phase Separation as a Molecular Thermosensor. Dev. Cell **55**:118-119. 10.1016/j.devcel.2020.09.019.

Li, J., Zhang, Z., Chong, K., and Xu, Y. (2022). Chilling tolerance in rice: Past and present. J. Plant Physiol. **268**:153576. 10.1016/j.jplph.2021.153576.

Li, W., Yan, J., Zhang, Y., Zhang, F., Guan, Z., Yao, Y., Chang, Y., Tu, H., Li, X., Wang, H., et al. (2023). Serine protease NAL1 exerts pleiotropic functions through degradation of TOPLESS-related corepressor in rice. Nat Plants 10.1038/s41477-023-01449-2.

Liu, C., Ou, S., Mao, B., Tang, J., Wang, W., Wang, H., Cao, S., Schlappi, M.R., Zhao, B., Xiao, G., et al. (2018). Early selection of bZIP73 facilitated adaptation of japonica rice to cold climates. Nat Commun **9**:3302. 10.1038/s41467-018-05753-w.

Liu, S., Liu, S., Wang, M., Wei, T., Meng, C., Wang, M., and Xia, G. (2014). A wheat SIMILAR TO RCD-ONE gene enhances seedling growth and abiotic stress resistance by modulating redox homeostasis and maintaining genomic integrity. Plant Cell **26**:164-180. 10.1105/tpc.113.118687.

Lu, G., Wu, F.Q., Wu, W., Wang, H.J., Zheng, X.M., Zhang, Y., Chen, X., Zhou, K., Jin, M., Cheng, Z., et al. (2014). Rice LTG1 is involved in adaptive growth and fitness under low ambient temperature. Plant J. **78**:468-480. 10.1111/tpj.12487.

Lv, Y., Guo, Z., Li, X., Ye, H., Li, X., and Xiong, L. (2016). New insights into the genetic basis of natural chilling and cold shock tolerance in rice by genome-wide association analysis. Plant Cell Environ **39**:556-570. 10.1111/pce.12635.

Ma, Q., Dai, X., Xu, Y., Guo, J., Liu, Y., Chen, N., Xiao, J., Zhang, D., Xu, Z., Zhang, X., et al. (2009). Enhanced Tolerance to Chilling Stress in OsMYB3R-2 Transgenic Rice Is Mediated by Alteration in Cell Cycle and Ectopic Expression of Stress Genes. Plant Physiol. **150**:244-256. 10.1104/pp.108.133454.

Ma, Y., Dai, X., Xu, Y., Luo, W., Zheng, X., Zeng, D., Pan, Y., Lin, X., Liu, H., Zhang, D., et al. (2015). COLD1 confers chilling tolerance in rice. Cell **160**:1209-1221. 10.1016/j.cell.2015.01.046.

Mao, D., Xin, Y., Tan, Y., Hu, X., Bai, J., Liu, Z.-y., Yu, Y., Li, L., Peng, C., Fan, T., et al. (2019). Natural variation in the HAN1 gene confers chilling tolerance in rice and allowed adaptation to a temperate climate. Proc Natl Acad Sci U S A **116**:3494-3501. 10.1073/pnas.1819769116.

Matsukura, S., Mizoi, J., Yoshida, T., Todaka, D., Ito, Y., Maruyama, K., Shinozaki, K., and Yamaguchi-Shinozaki, K. (2010). Comprehensive analysis of rice DREB2-type genes that encode transcription factors involved in the expression of abiotic stress-responsive genes. Mol. Genet. Genomics **283**:185-196. 10.1007/s00438-009-0506-y.

Nakashima, K., Tran, L.-S.P., Van Nguyen, D., Fujita, M., Maruyama, K., Todaka, D., Ito, Y., Hayashi, N., Shinozaki, K., and Yamaguchi-Shinozaki, K. (2007). Functional analysis of a NAC-type transcription factor OsNAC6 involved in abiotic and biotic stress-responsive gene expression in rice. Plant J. **51**:617-630. 10.1111/j.1365-313X.2007.03168.x.

Noguchi, M., and Kodama, Y. (2022). Temperature Sensing in Plants: On the Dawn of Molecular Thermosensor Research. Plant Cell Physiol. **63**:737-743. 10.1093/pcp/pcac033.

Patel, A., Lee, H.O., Jawerth, L., Maharana, S., Jahnel, M., Hein, M.Y., Stoynov, S., Mahamid, J., Saha, S., Franzmann, T.M., et al. (2015). A Liquid-to-Solid Phase Transition of the ALS Protein FUS Accelerated by Disease Mutation. Cell **162**:1066-1077. 10.1016/j.cell.2015.07.047.

Pertea, M., Kim, D., Pertea, G.M., Leek, J.T., and Salzberg, S.L. (2016). Transcript-level expression analysis of RNA-seq experiments with HISAT, StringTie and Ballgown. Nat Protoc **11**:1650-1667. 10.1038/nprot.2016.095.

Pertea, M., Pertea, G.M., Antonescu, C.M., Chang, T.C., Mendell, J.T., and Salzberg, S.L. (2015). StringTie enables improved reconstruction of a transcriptome from RNA-seq reads. Nat. Biotechnol. **33**:290-295. 10.1038/nbt.3122.

Qin, L., Sun, L., Wei, L., Yuan, J., Kong, F., Zhang, Y., Miao, X., Xia, G., and Liu, S. (2021). Maize SRO1e represses anthocyanin synthesis through regulating the MBW complex in response to abiotic stress. Plant J. **105**:1010-1025. 10.1111/tpj.15083.

Silva, C.S., Nayak, A., Lai, X., Hutin, S., Hugouvieux, V., Jung, J.-H., López-Vidriero, I., Franco-Zorrilla, J.M., Panigrahi, K.C.S., Nanao, M.H., et al. (2020). Molecular mechanisms of Evening Complex activity in Arabidopsis. Proc Natl Acad Sci U S A **117**:6901-6909. 10.1073/pnas.1920972117.

Soualiou, S., Duan, F., Li, X., and Zhou, W. (2022). CROP PRODUCTION UNDER COLD STRESS: An understanding of plant responses, acclimation processes, and management strategies. Plant Physiol. Biochem. **190**:47-61. 10.1016/j.plaphy.2022.08.024.

Vainonen, J.P., Gossens, R., Krasensky-Wrzaczek, J., De Masi, R., Danciu, I., Puukko, T., Battchikova, N., Jonak, C., Wirthmueller, L., Wrzaczek, M., et al. (2023). Poly(ADP-ribose)-binding protein RCD1 is a plant PARylation reader regulated by Photoregulatory Protein Kinases. Commun Biol **6**:429. 10.1038/s42003-023-04794-2.

Waadt, R., Schmidt, L.K., Lohse, M., Hashimoto, K., Bock, R., and Kudla, J. (2008). Multicolor bimolecular fluorescence complementation reveals simultaneous formation of alternative CBL/CIPK complexesin planta. Plant J. **56**:505-516. 10.1111/j.1365-313X.2008.03612.x.

Wang, L., Cheng, H., Wang, Q., Si, C., Yang, Y., Yu, Y., Zhou, L., Ding, L., Song, A., Xu, D., et al. (2021). CmRCD1 represses flowering by directly interacting with CmBBX8 in summer chrysanthemum. Hortic Res **8**:79. 10.1038/s41438-021-00516-z.

Wang, M., Wang, M., Zhao, M., Wang, M., Liu, S., Tian, Y., Moon, B., Liang, C., Li, C., Shi, W., et al. (2022). TaSRO1 plays a dual role in suppressing TaSIP1 to

fine tune mitochondrial retrograde signaling and enhance salinity stress tolerance. New Phytol. **236**:495-511. 10.1111/nph.18340.

Wang, W., Mauleon, R., Hu, Z., Chebotarov, D., Tai, S., Wu, Z., Li, M., Zheng, T., Fuentes, R.R., Zhang, F., et al. (2018). Genomic variation in 3,010 diverse accessions of Asian cultivated rice. Nature **557**:43-49. 10.1038/s41586-018-0063-9.

Wang, Y., He, S., and Fang, X. (2023). Emerging roles of phase separation in plant transcription and chromatin organization. Curr. Opin. Plant Biol. **75**:102387. 10.1016/j.pbi.2023.102387.

Xie, K., and Yang, Y. (2013). RNA-Guided Genome Editing in Plants Using a CRISPR–Cas System. Mol Plant **6**:1975-1983. 10.1093/mp/sst119.

Xie, K., Minkenberg, B., and Yang, Y. (2015). Boosting CRISPR/Cas9 multiplex editing capability with the endogenous tRNA-processing system. Proc Natl Acad Sci U S A **112**:3570-3575. 10.1073/pnas.1420294112.

Xue, W., Xing, Y., Weng, X., Zhao, Y., Tang, W., Wang, L., Zhou, H., Yu, S., Xu, C., Li, X., et al. (2008). Natural variation in Ghd7 is an important regulator of heading date and yield potential in rice. Nat. Genet. **40**:761-767. 10.1038/ng.143.

You, J., Zong, W., Du, H., Hu, H., and Xiong, L. (2014). A special member of the rice SRO family, OsSRO1c, mediates responses to multiple abiotic stresses through interaction with various transcription factors. Plant Mol. Biol. **84**:693-705. 10.1007/s11103-013-0163-8.

You, J., Zong, W., Li, X., Ning, J., Hu, H., Li, X., Xiao, J., and Xiong, L. (2013). The SNAC1-targeted gene OsSRO1c modulates stomatal closure and oxidative stress tolerance by regulating hydrogen peroxide in rice. J. Exp. Bot. **64**:569-583. 10.1093/jxb/ers349.

Yu, G., Wang, L.-G., Han, Y., and He, Q.-Y. (2012). clusterProfiler: an R Package for Comparing Biological Themes Among Gene Clusters. OMICS: J. Integrative Biol. **16**:284-287. 10.1089/omi.2011.0118.

Zamudio, A.V., Dall'Agnese, A., Henninger, J.E., Manteiga, J.C., Afeyan, L.K., Hannett, N.M., Coffey, E.L., Li, C.H., Oksuz, O., Sabari, B.R., et al. (2019). Mediator Condensates Localize Signaling Factors to Key Cell Identity Genes. Mol. Cell **76**:753-766.e756. 10.1016/j.molcel.2019.08.016.

Zhang, H., Zhu, J., Gong, Z., and Zhu, J.-K. (2022). Abiotic stress responses in plants. Nat. Rev. Genet. **23**:104-119. 10.1038/s41576-021-00413-0.

Zhang, Z., Li, J., Pan, Y., Li, J., zhou, L., Shi, H., Zeng, Y., Guo, H., Yang, S., Zheng, W., et al. (2017). Natural variation in CTB4a enhances rice adaptation to cold habitats. Nat Commun **8**:14788. 10.1038/ncomms14788.

Zhao, H., Li, J., Yang, L., Qin, G., Xia, C., Xu, X., Su, Y., Liu, Y., Ming, L., Chen, L.-L., et al. (2021). An inferred functional impact map of genetic variants in rice. Mol Plant **14**:1584-1599. 10.1016/j.molp.2021.06.025.

Zhou, Z., Bi, G., and Zhou, J.M. (2018). Luciferase Complementation Assay for Protein-Protein Interactions in Plants. Curr Protoc Plant Biol **3**:42-50. 10.1002/cppb.20066.

Zhu, J.K. (2016). Abiotic Stress Signaling and Responses in Plants. Cell **167**:313-324. 10.1016/j.cell.2016.08.029.

Zhu, P., Lister, C., and Dean, C. (2021). Cold-induced Arabidopsis FRIGIDA nuclear condensates for FLC repression. Nature **599**:657-661. 10.1038/s41586-021-04062-5.

Zhu, S., Gu, J., Yao, J., Li, Y., Zhang, Z., Xia, W., Wang, Z., Gui, X., Li, L., Li, D., et al. (2022). Liquid-liquid phase separation of RBGD2/4 is required for heat stress resistance in Arabidopsis. Dev. Cell **57**:583-597 e586. 10.1016/j.devcel.2022.02.005.

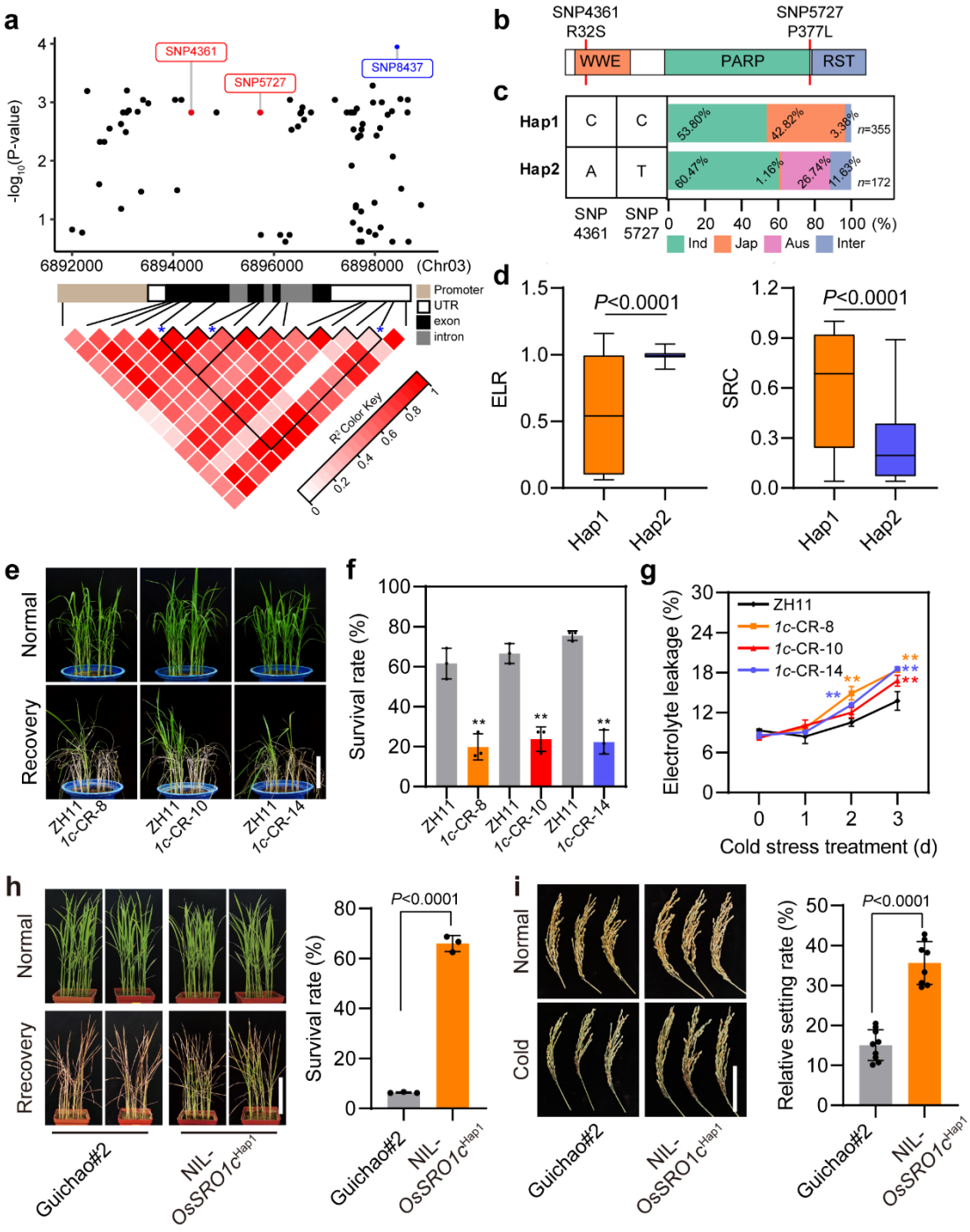

Fig. 1 *OsSRO1c* is associated with cold tolerance in rice.

a, *OsSRO1c* association mapping and pairwise linkage disequilibrium (LD) analysis. Top, Manhattan plot of association analysis in *OsSRO1c* locus and electrolyte leakage after recovery (ELR) for 7 d traits. The *OsSRO1c* physical location is shown on the x-axis. The lead SNP is shown as a blue dot, and the two non-synonymous SNPs are in

red. Bottom, LD diagram of the representative SNPs including two non-synonymous SNPs and the lead SNP indicated by blue asterisks.

b, Schematic diagram of the protein domain of OsSRO1c. The red lines indicate the positions of the two non-synonymous variants.

c, Haplotypes and subpopulation composition of *OsSRO1c* identified in the natural variation. *n* denotes the number of germplasms in each haplotype group.

d, Comparison of ELR and survival rate after natural chilling stress (SRC) between Hap1 and Hap2. For the boxplots, the center line indicates the median, the edges of the box represent the first and third quartiles, the whiskers extend to 1.5 times interquartile range from the box edges. (n = 269 and 121 varieties for ELR, n = 226 and 78 varieties for SRC). Significance was determined by unpaired two-tailed Student's *t*-test.

e, Photographs of the wild-type rice Zhonghua11 (ZH11) and three independent *ossro1c* mutant lines (*1c*-CR-8, *1c*-CR-10 and *1c*-CR-14) at four-leaf stage under normal condition and after recovery from cold stress. Scale bars, 10 cm.

f, Survival rates of the plants in (**e**) after recovery from cold stress treatment. Data represent as mean ± SD (n = 3 biological replicates). Significance was determined by unpaired two-tailed Student's *t*-test (** $P < 0.01$).

g, Leaf electrolyte leakage of the plants in (**e**) under normal condition and during cold stress treatment. Data represent as mean ± SD (n = 3 biological replicates). Asterisks represent significant differences compared with ZH11 by one-way ANOVA (** $P < 0.01$).

h, Photographs (left) and survival rate (right) of Guichao#2 and NIL-*OsSRO1c*^{Hap1} plants at four-leaf stage under normal condition and after recovery from cold stress. Scale bars, 10 cm. Data represent as mean ± SD (n = 3 biological replicates). Significance was determined by unpaired two-tailed Student's *t*-test.

i, Representative spike photographs (left) and relative setting rate (right) of Guichao#2 and NIL-*OsSRO1c*^{Hap1} plants under normal condition and after cold stress. Scale bars,

10 cm. Data represent as mean ± SD (n = 3 biological replicates). Significance was determined by unpaired two-tailed Student's t-test.

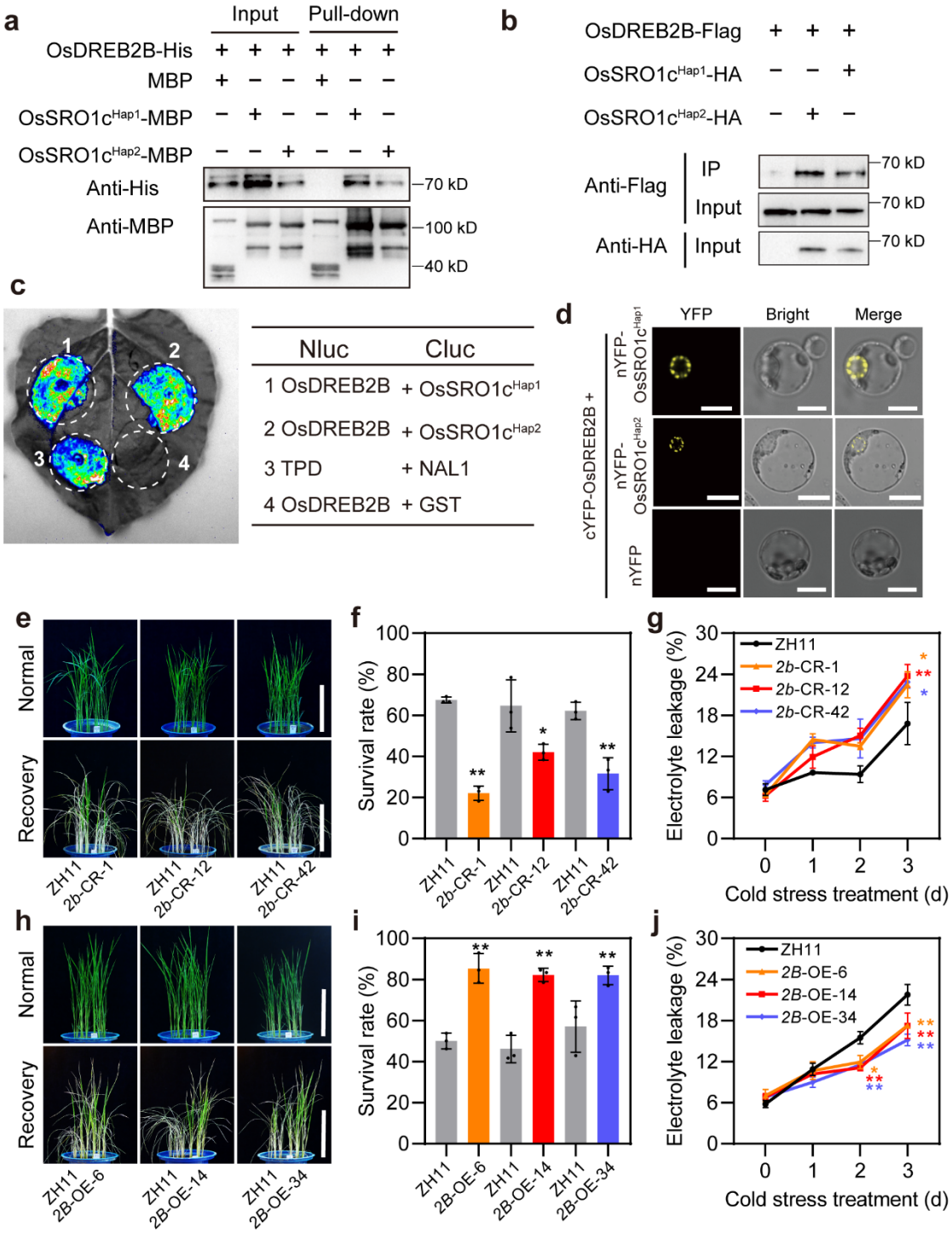

Fig. 2 OsSRO1c variants interact with cold stress positive regulator OsDREB2B.

a, *In vitro* pull-down assay. OsSRO1c^{Haps}-MBP fusion protein or MBP alone was incubated with OsDREB2B-His in MBP beads. OsDREB2B-His was pulled down by OsSRO1c^{Haps}-MBP but not MBP. Western blot was used with anti-MBP and anti-His antibody.

b, *In vivo* co-immunoprecipitation (Co-IP) assay. OsSRO1c^{Haps}-HA or the HA tag was co-transformed with OsDREB2B-Flag in rice protoplasts. Total protein was extracted from the rice protoplasts and incubated with HA beads. OsDREB2B-Flag was co-immunoprecipitation by OsSRO1c^{Haps}-HA but not HA tag alone. Western blot was used with anti-Flag and anti-HA antibodies.

c, *In vivo* luciferase complementation assay in tobacco. OsDREB2B was fused with the N-terminal half of luciferase (Nluc), while OsSRO1c^{Haps} were fused with the C-terminal half of luciferase (Cluc). Interaction between the N terminus of OsTPR2 (TPD) and NAL1 was used as a positive control (Li et al., 2023). Interaction between the OsDREB2B and GST was used as a negative control.

d, Representative images of BiFC assay results in rice protoplasts under normal condition. Scale bars, 10 μm.

e,h Photographs of the wild-type rice Zhonghua11 (ZH11) and three independent *osdreb2b* mutant lines (*2b*-CR-1, *2b*-CR-12, and *2b*-CR-42) (**e**) or ZH11 and three independent *OsDREB2B* overexpression transgenic rice lines (*2B*-OE-6, *2B*-OE-14 and *2B*-OE-34) (**h**) at four-leaf stage under normal condition and after recovery from cold stress. Scale bars, 10 cm.

f,i Survival rate of ZH11 and *osdreb2b* mutant lines (**f**) or ZH11 and *OsDREB2B* OE lines (**i**) after recovery from cold stress treatment. Data represent as mean ± SD (n = 3 biological replicates). Significance was determined by unpaired two-tailed Student's t-test (* $P < 0.05$, ** $P < 0.01$).

g,j Leaf electrolyte leakage of ZH11 and *osdreb2b* mutant lines (**g**) or ZH11 and *OsDREB2B* OE lines (**j**) under normal condition and during cold stress treatment. Data represent as mean ± SD (n = 3 biological replicates). Asterisks represent significant differences compared with ZH11 by one-way ANOVA (* $P < 0.05$, ** $P < 0.01$).

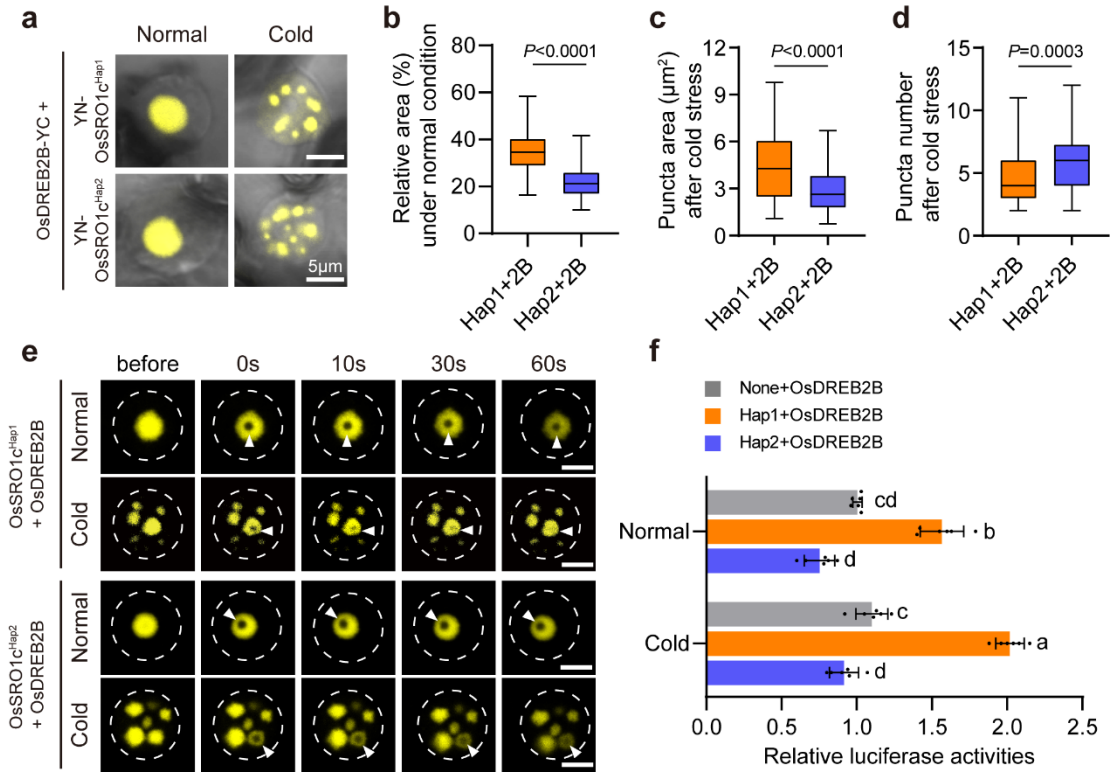

Fig. 3 OsSRO1c^{Haps}-OsDREB2B complexes form distinct condensates that modulate OsDREB2B activity.

a, Representative images of BiFC assay results in tobacco leaves under both normal and cold stress conditions. Scale bars, 5 μm.

b, The relative area of condensate to the nucleus in two haplotype complexes under normal condition (n = 100 and 100 cells). Significance was determined by unpaired two-tailed Student's t-test.

c,d The average puncta area (**c**) and the puncta number per nucleus (**d**) in two haplotype complexes after cold stress. (n = 100 and 100 cells in c,d). Significance was determined by unpaired two-tailed Student's t-test. For the boxplots in b-d, the center line indicates the median, the edges of the box represent the first and third quartiles, the whiskers extend to 1.5 times interquartile range from the box edges.

e, Images of FRAP in OsSRO1c^{Hap1}-OsDREB2B complex (top) and OsSRO1c^{Hap2}-OsDREB2B complex (down) granules under both normal and cold stress conditions respectively. Dotted white circles represent the nucleus. White triangles indicate bleached areas. Scale bars, 5 μm.

f, Dual luciferase (LUC) reporter assays under both normal and cold stress conditions. Data represent as mean ± SD (n = 6 biological replicates). Different lowercase letters above bars indicate a significant difference at the $P < 0.05$ level by one-way ANOVA.

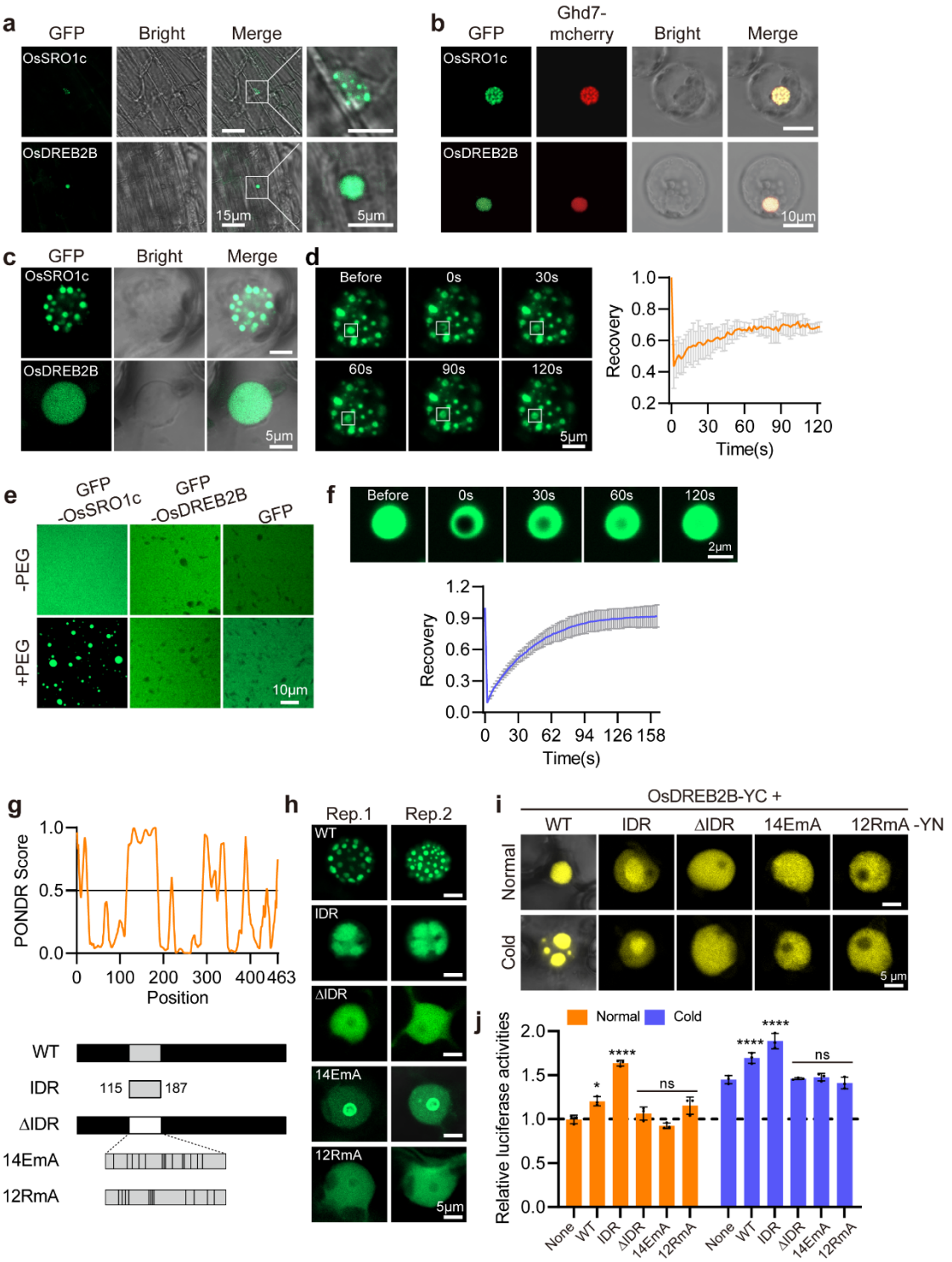

Fig. 4 OsSRO1c undergoes LLPS *in vivo* and *in vitro*.

a, OsSRO1c and OsDREB2B protein signal (puncta or diffuse) in rice root-tip nuclei under normal condition, respectively. Scale bars, 15 μm (left), 5 μm (right).

b, OsSRO1c and OsDREB2B protein signal in rice protoplasts under normal condition, respectively. GFP signal of OsSRO1c or OsDREB2B was merged with that of the

Ghd7-mCherry (an intrinsic nuclear protein) marker in rice protoplasts. Scale bars, 10 μm.

c, OsSRO1c and OsDREB2B protein signal in tobacco leaves under normal condition. Scale bars, 5 μm.

d, Representative granule images of FRAP (left) and recovery curve (right) of OsSRO1c in tobacco leaves. White squares indicate bleached granules. Scale bars, 5 μm. Data represent as mean ± SD (n = 3 biological replicates).

e, *In vitro* phase-separation assays of GFP-OsSRO1c, GFP-OsDREB2B and GFP protein with 5% (w/v) PEG 6,000 treatment for 5 min. Scale bars, 5 μm.

f, OsSRO1c droplets *in vitro* display liquid-like property. Representative droplets images of FRAP (top) and recovery curve (bottom) of GFP-OsSRO1c. Scale bars, 2 μm. Data represent as mean ± SD (n = 3).

g, Intrinsically disordered regions (IDRs) prediction curve (top, analyzed by "Predictor of Natural Disordered Regions" PONDR; http://www.pondr.com/) and schematic diagrams of OsSRO1c variants (bottom). Grey box represents the IDR. Black lines indicate the positions of charged amino acid Glu and Arg mutated to Ala in the IDR, respectively.

h, Two representative images of protein signal of mutant versions of OsSRO1c in tobacco leaves. Scale bars, 5 μm.

i, Representative images of BiFC assay results in tobacco leaf under both normal and cold stress conditions. Scale bars, 5 μm.

j, Dual luciferase (LUC) reporter assays of mutated OsSRO1c on transcriptional activity of OsDREB2B under both normal and cold stress conditions. Data represent as mean ± SD (n = 3 biological replicates). Significance was determined by one-way ANOVA (* $P < 0.05$, **** $P < 0.0001$, ns, no significant). OsSRO1c^{Hap1} was used in the whole Fig. 4.

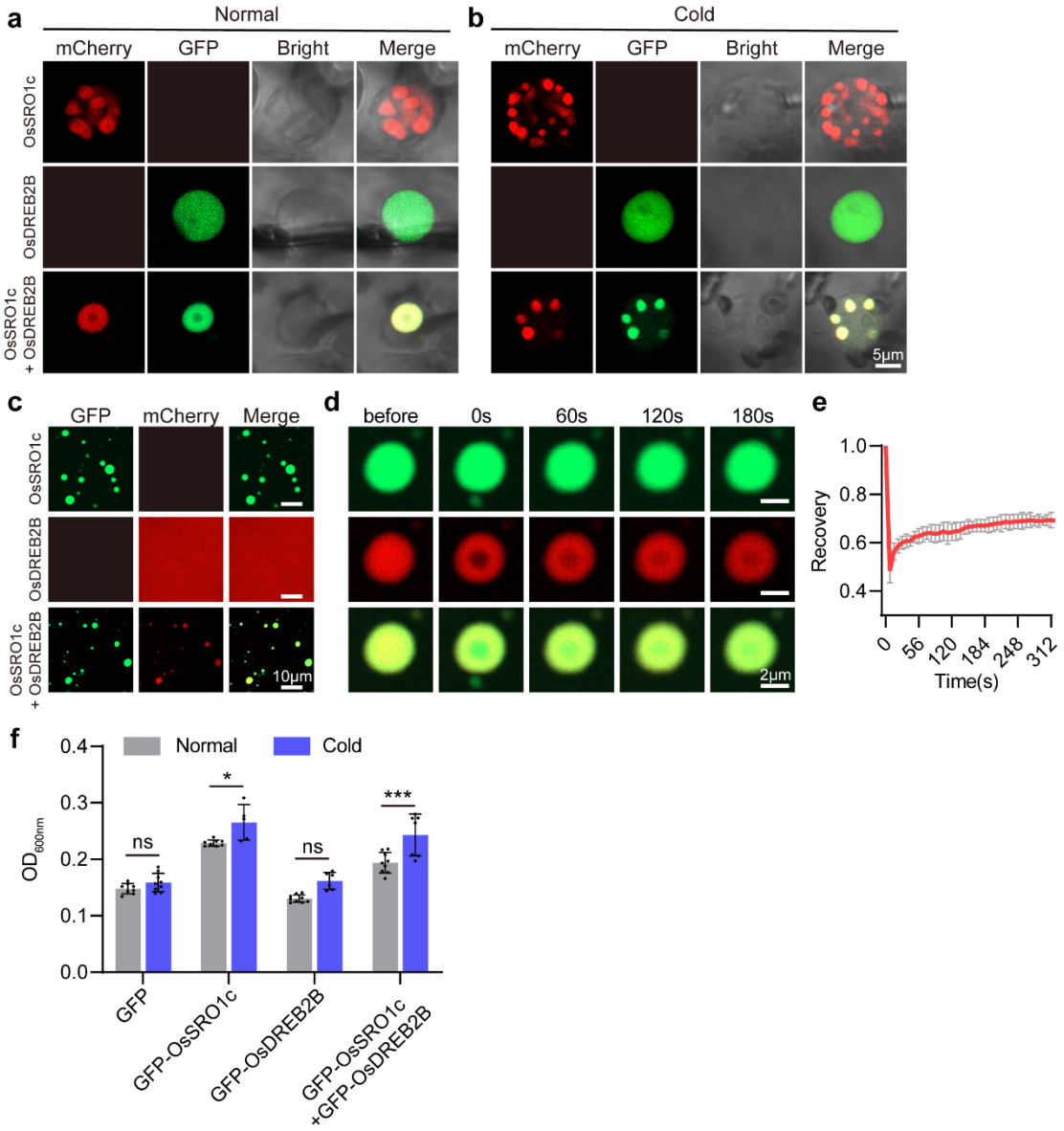

Fig. 5 OsSRO1c-OsDREB2B complex undergoes dynamic phase transition under cold stress *in vivo* and *in vitro*.

a,b Representative confocal images of OsSRO1c-mCherry alone, OsDREB2B-GFP alone, and OsSRO1c-mCherry and OsDREB2B-GFP complex in tobacco leaves under normal (**a**) and cold stress (**b**). Scale bars, 5 μm.

c, GFP-OsSRO1c and mCherry-OsDREB2B co-condense *in vitro*. Scale bars, 10 μm.

d, Representative FRAP images of the OsSRO1c-mCherry and OsDREB2B-GFP complex co-condensates *in vitro*.

e, FRAP recovery curve (down). Scale bars, 2 μm. Data represent as mean ± SD (n = 3).

f, Turbidity measurement of GFP, GFP-OsSRO1c, and GFP-OsDREB2B and GFP-OsSRO1c-GFP-OsDREB2B complex under both normal and cold stress conditions. Data represent as mean ± SD (n = 9). Significance was determined by unpaired two-tailed Student's t-test (* $P < 0.05$, **** $P < 0.0001$, ns, no significant).

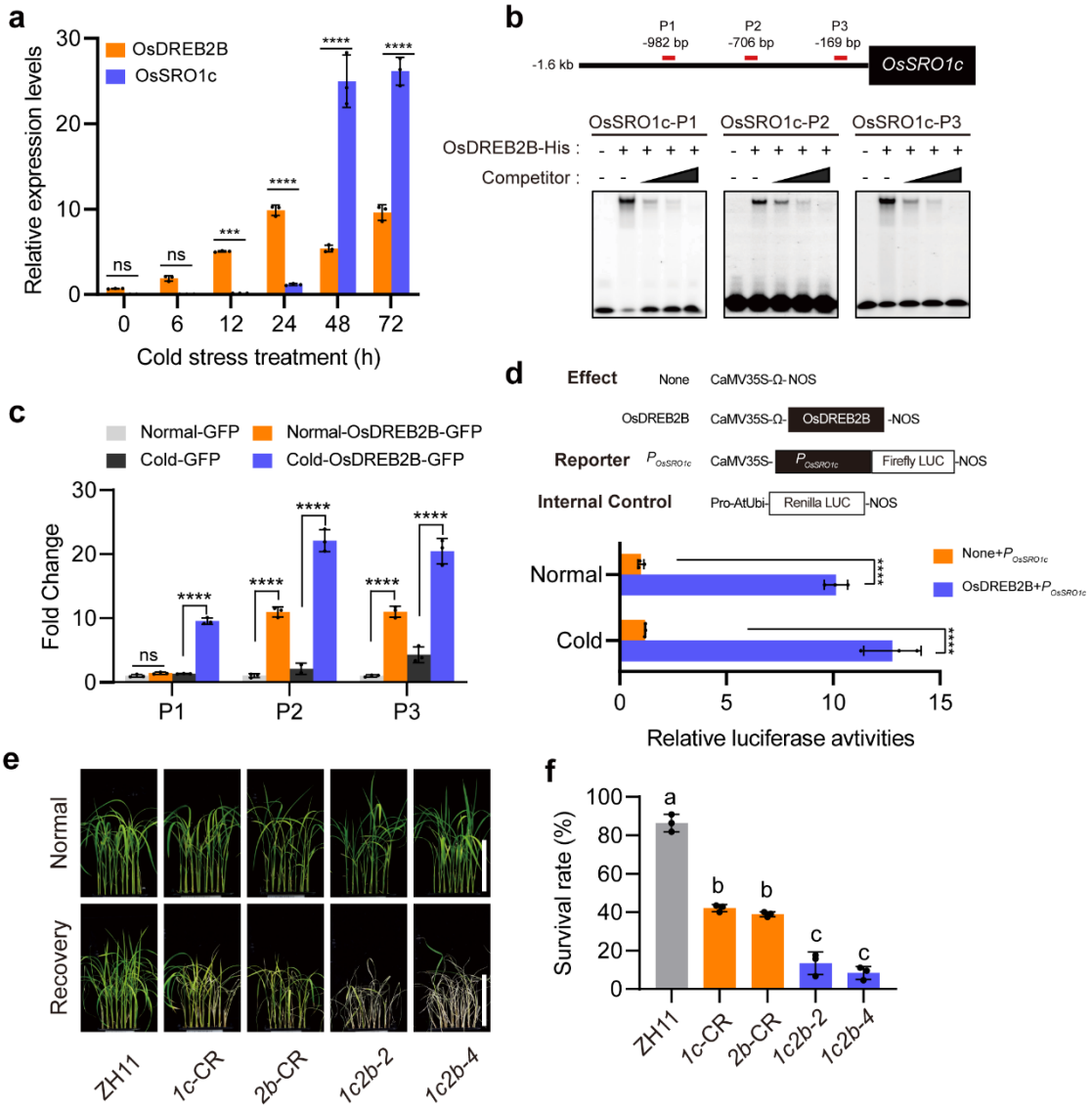

Fig. 6 OsDREB2B is a positively regulator of *OsSRO1c*.

a, Relative expression levels of *OsSRO1c* and *OsDREB2B* in ZH11 plants during cold stress. Data represent as mean ± SD (n = 3). Significance was determined by unpaired two-tailed Student's t-test (*** $P < 0.001$, **** $P < 0.0001$, ns, no significant).

b, EMSA showing that OsDREB2B binds to the conserved DRE elements of the *OsSRO1c* promoter. Top, Schematic diagrams of the *OsSRO1c* promoter. The red lines indicate the position of the DRE elements.

c, ChIP-qPCR assay showing that OsDREB2B binds to the promoter of *OsSRO1c in vivo*. Immunoprecipitation was performed with anti-GFP antibody. qPCR enrichment was calculated by normalizing to the GFP empty vector transformation. Data represent

as mean ± SD (n = 3). Significance was determined by unpaired two-tailed Student's t-test (**** $P < 0.0001$, ns, no significant).

d, Dual luciferase (LUC) reporter assay in rice protoplasts showing that OsDREB2B promotes the transcription of *OsSRO1c* under both normal and cold stress conditions. Top, Schematic diagrams of the effector and reporter plasmids. Data represent as mean ± SD (n = 3). Significance was determined by unpaired two-tailed Student's t-test (**** $P < 0.0001$).

e, Photograph of ZH11, *ossro1c* mutants (*1c*-CR), *osdreb2b* mutants (*2b*-CR) and *ossro1c osdreb2b* double mutant lines (*1c2b-2* and *1c2b-4*) at four-leaf stage under normal condition and after recovery from cold stress. Scale bars, 10 cm.

f, Survival rate of the plants in (**e**) after recovery from cold stress treatment. Data represent as mean ± SD (n = 3). Different lowercase letters above bars indicate a significant difference at the $P < 0.05$ level by one-way ANOVA.

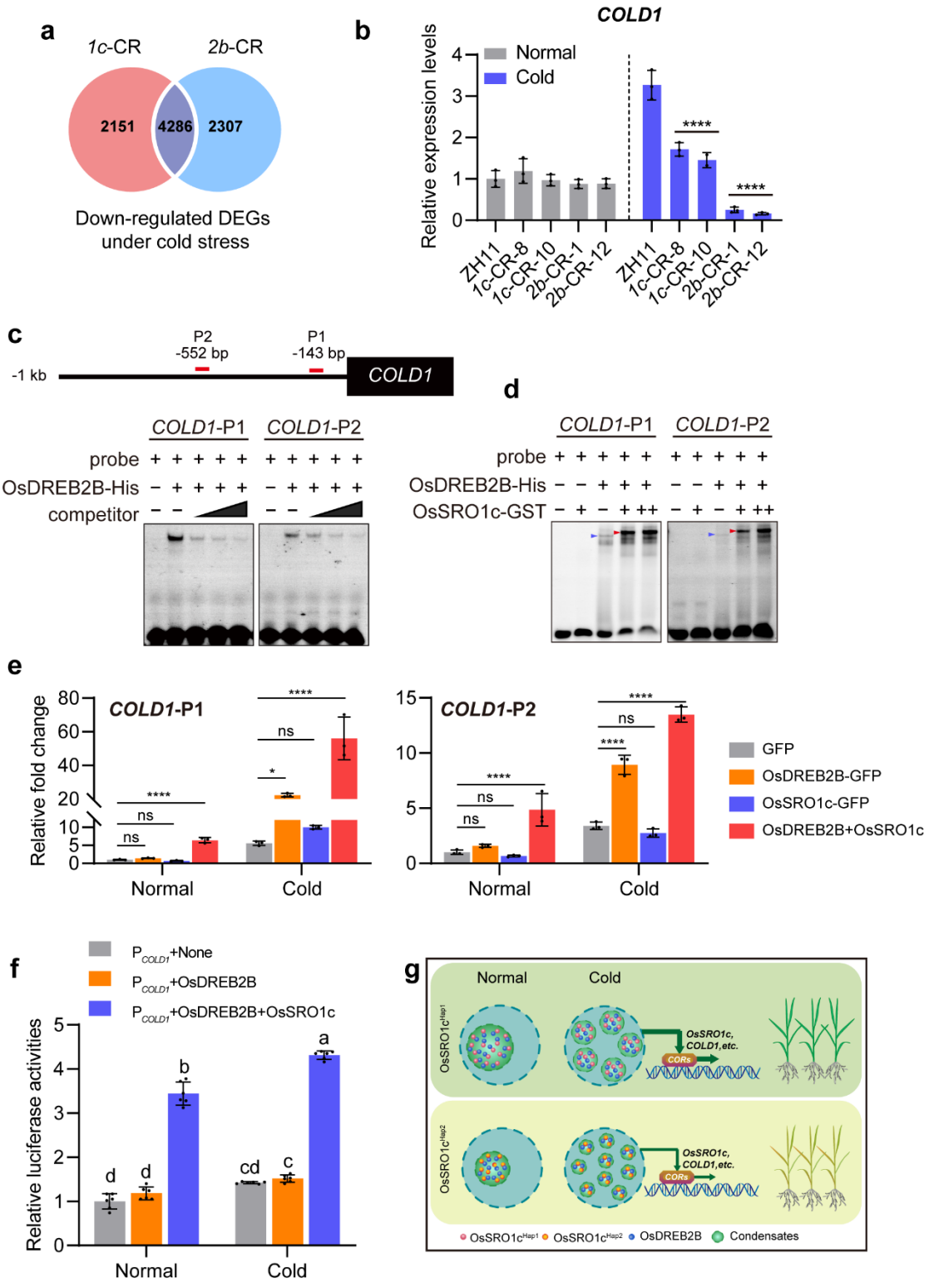

Fig. 7 *COLD1* is a direct target gene of the OsSRO1c-OsDREB2B complex.

a, Venn diagrams showing the number of down-regulated DEGs in 1*c*-CR (left) or *2b*-CR (right) compared with ZH11 under cold stress, respectively.

b, The relative expression levels of *COLD1* in *1c*-CR, *2b*-CR and ZH11 based on RNA-seq data. Data represent as mean ± SD (n = 3). Asterisks represent significant differences compared with ZH11 by one-way ANOVA (**** $P < 0.0001$).

c, EMSA assays showing the binding of OsDREB2B to the promoters of *COLD1 in vitro.*

d, EMSA assays showing the binding of OsSRO1c-OsDREB2B complex to the promoters of *COLD1 in vitro.* Blue triangles indicate the binding band of OsDREB2B alone to the DNA probes, red triangles indicate the supershifted band, showing the binding of the OsSRO1c-OsDREB2B complex to the DNA probes.

e, ChIP-qPCR assay showing that OsDREB2B binds to the promoter of *COLD1 in vivo*. Immunoprecipitation was performed with anti-GFP antibody. qPCR enrichment was calculated by normalizing to the GFP empty vector transformation. Data represent as mean ± SD (n = 3). Asterisks represent significant differences compared with GFP by one-way ANOVA (* $P < 0.05$, **** $P < 0.0001$, ns, no significant).

f, Dual luciferase (LUC) reporter assay in rice protoplasts showing that OsSRO1c-OsDREB2B complex promotes the transcription of *COLD1* under both normal and cold stress conditions. Data represent as mean ± SD (n = 6). Different lowercase letters above bars indicate a significant difference at the $P < 0.05$ level by one-way ANOVA.

g, Working model of the role of OsSRO1c-OsDREB2B complex in the regulation of cold tolerance.

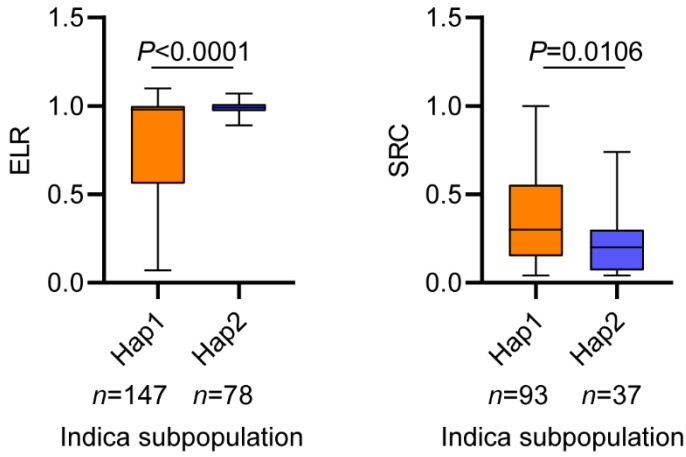

Extended Data Fig. 1 The differences of ELR and SRC traits between two haplotypes in *indica* subpopulation.

Boxplots of electrolyte leakage after recovery (ELR) for 7 d traits and survival rate after natural chilling stress (SRC) traits distribution of two haplotypes in *indica* subpopulation. Data represent from 5-95 percentile (Student's *t* test, n = 147 and 78, n = 93 and 37).

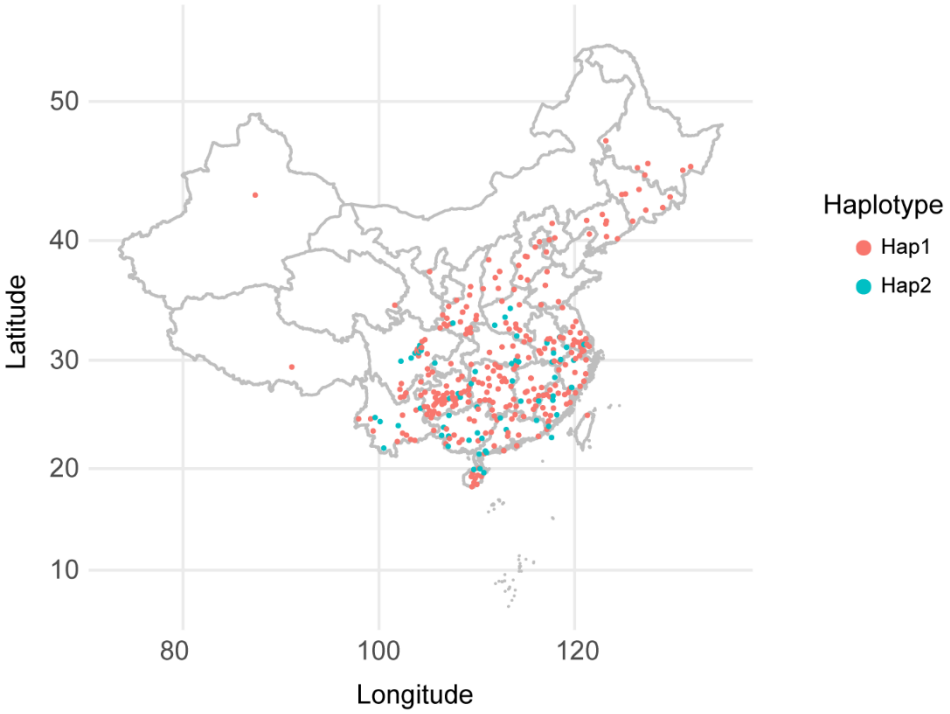

Extended Data Fig. 2 Geographical distribution of OsSRO1c^{Haps} in rice germplasms from China.

Geographical distribution of the two haplotypes of *OsSRO1c* in China. The orange points indicate the Hap1 varieties and the blue points indicate the Hap2 varieties.

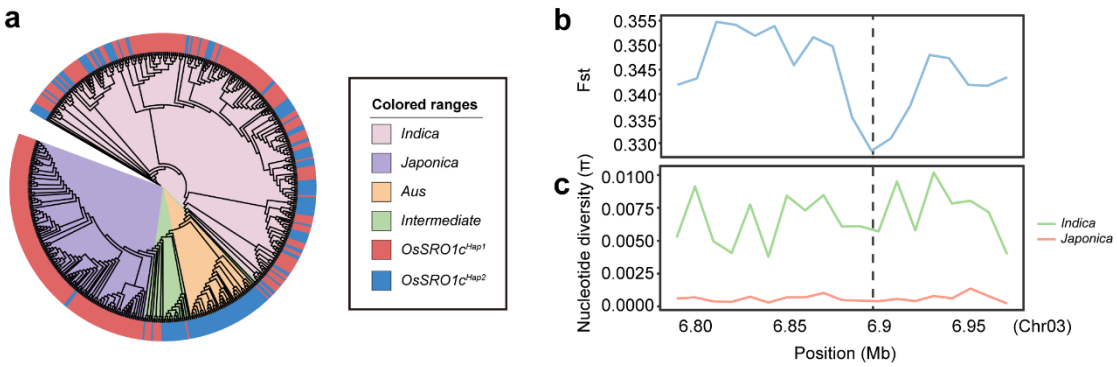

Extended Data Fig. 3 Genetic analysis of natural variation in *OsSRO1c*

a. Phylogram of *OsSRO1c* generated from 527 diverse rice accessions showing the divergence between *indica* and *japonica*.

b & c. *Fst* (b) and nucleotide diversity (π) (c) analysis across the 150-kb genomic region containing the *OsSRO1c* locus. The black dotted vertical line indicates the location of the *OsSRO1c* gene.

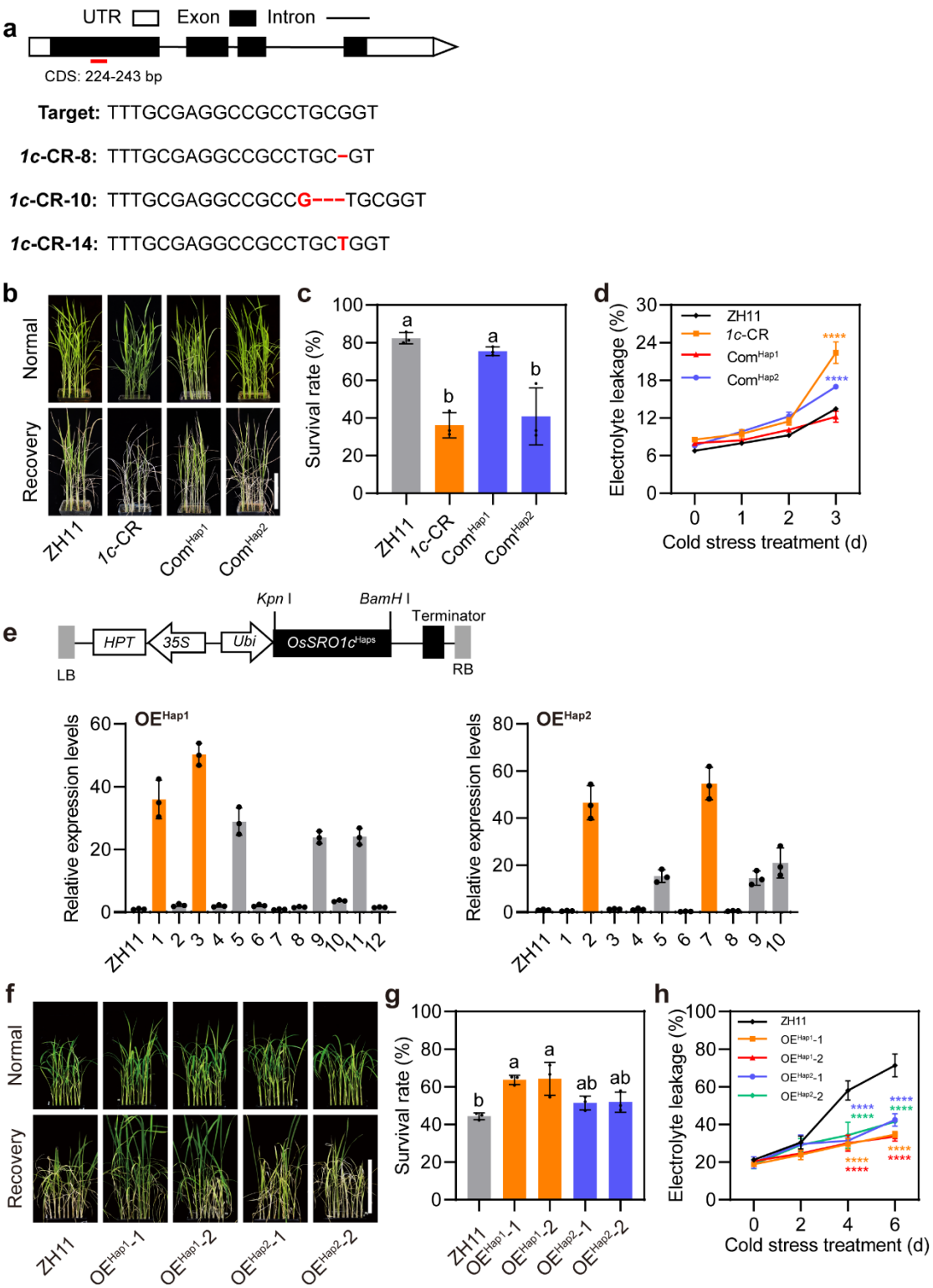

Extended Data Fig. 4 Phenotype of *OsSRO1c* transgenic plants after cold stress treatment.

a, Gene structure and mutation sites in *OsSRO1c*. Mutation sites are indicated with red lines.

b,c&d Photographs **(b)**, survival rate **(c)** and leaf electrolyte leakage **(d)** of the wild-type rice Zhonghua11 (ZH11), *ossro1c* mutants (*1c*-CR) and two haplotypes of *OsSRO1c* complementary lines (Com^{Hap1} and Com^{Hap2}) at four-leaf stage under normal condition and after recovery from cold stress.

e, Schematic diagram of the construct over-expressing $OsSRO1c^{Haps}$ (up) and expression analysis of $OsSRO1c^{Haps}$ in $OsSRO1c^{Haps}$ over-expression transgenic rice lines (OE^{Hap1} and OE^{Hap2}) using qRT-PCR analysis (down). The over-expression lines used for further analysis are labeled in orange. Data represent as mean ± SD of three replicates.

f,g&h Photographs **(f)**, survival rate **(g)** and leaf electrolyte leakage **(h)** of ZH11 and two haplotypes of *OsSRO1c* over-expression transgenic rice lines (OE^{Hap1} and OE^{Hap2}) at four-leaf stage under normal condition and after recovery from cold stress.

b&f Scale bars, 10 cm. **c&g,** Data represent as mean ± SD ($n = 3$). Different lowercase letters above bars indicate a significant difference at the $P < 0.05$ level by one-way ANOVA. **d&h,** Data represent as mean ± SD ($n = 3$). Asterisks represent significant differences compared with ZH11 by one-way ANOVA (**** $P < 0.0001$).

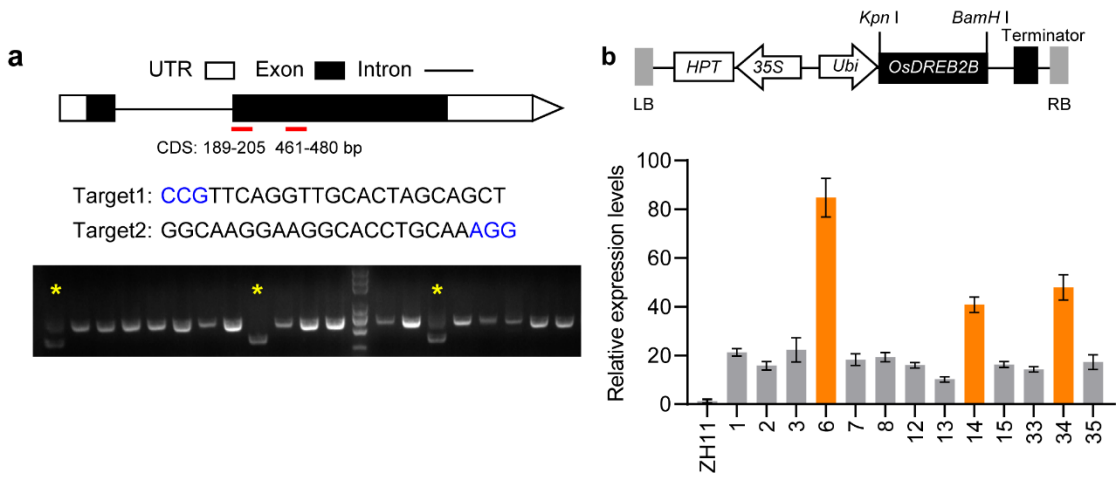

Extended Data Fig. 5 Confirmation of *OsDREB2B* knockout mutant and over-expression lines.

a, Gene structure and mutation sites in *OsDREB2B* (up) and DNA gel image for *osdreb2b* mutant genotyping (down). Mutation sites are indicated with red lines. The blue letters represent the PAM sequence. The mutant lines used for further analysis are labeled in yellow asterisk.

b, Schematic diagram of the construct over-expressing *OsDREB2B* (up) and expression analysis of *OsDREB2B* in *OsDREB2B*-OE transgenic plants using qRT-PCR analysis (down). The overexpression lines used for further analysis are labeled in orange. Data represent as mean ± SD of three replicates.

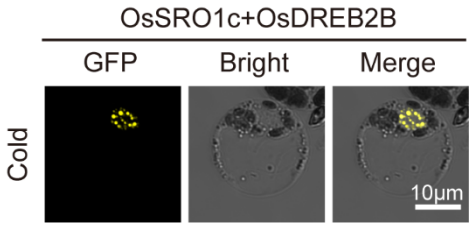

Extended Data Fig. 6 Localization of OsSRO1c-OsDREB2B complex in rice protoplasts after cold stress.

Localization of OsSRO1c-OsDREB2B complex in rice protoplasts after cold stress (4℃ for 2 h). Scale bars, 10 μm.

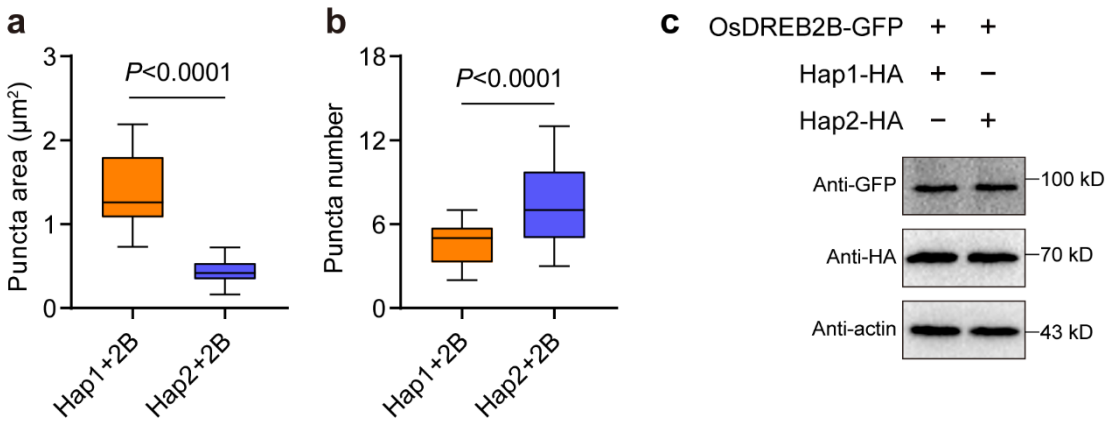

Extended Data Fig. 7 Statistical analysis of puncta area, puncta number and protein levels in OsSRO1c^{Haps}-OsDREB2B complex under normal condition.

a,b Quantification of the puncta area **(a)** and number **(b)** of OsSRO1c^{Haps}-OsDREB2B complex per cell in rice protoplasts under normal condition. For the boxplots, the center line indicates the median, the edges of the box represent the first and third quartiles, the whiskers extend to 1.5 times interquartile range from the box edges. (n = 30 and 30 in a, n = 28 and 29 in b). Significance was determined by unpaired two-tailed Student's t-test.

c, Western blot showed the total protein levels of OsSRO1c^{Haps} and OsDREB2B in the OsSRO1c^{Haps}-OsDREB2B complex in rice protoplasts under normal condition. GFP antibody is used to detect the protein levels of OsDREB2B-GFP, HA antibody is used to detect the protein levels of OsSRO1c^{Haps}-HA and plant specific actin antibody is used to evaluate the equal sample loading.

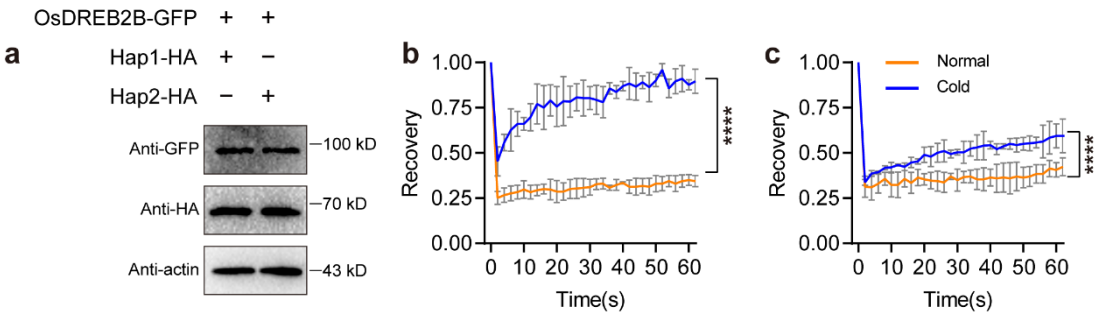

Extended Data Fig. 8 Co-condensates of the OsSRO1c^{Haps}-OsDREB2B complexes show distinct dynamics *in vivo*.

a, Detection of protein levels in OsSRO1c^{Haps}-OsDREB2B complex in tobacco leaves under normal conditions. Western blot showed the total protein levels of OsSRO1c^{Haps} and OsDREB2B in the OsSRO1c^{Haps}-OsDREB2B complex in tobacco leaves. GFP antibody is used to detect the protein levels of OsDREB2B-GFP, HA antibody is used to detect the protein levels of OsSRO1c^{Haps}-HA and plant specific actin antibody is used to evaluate the equal sample loading.

b & c, FRAP recovery curves of OsSRO1c^{Hap1}-OsDREB2B complex **(b)** and OsSRO1c^{Hap2}-OsDREB2B complex **(c)** in tobacco leaves under both normal and cold stress conditions. Data represent as mean ± SD (n = 3). Significance was determined by unpaired two-tailed Student's t-test (**** $P < 0.0001$).

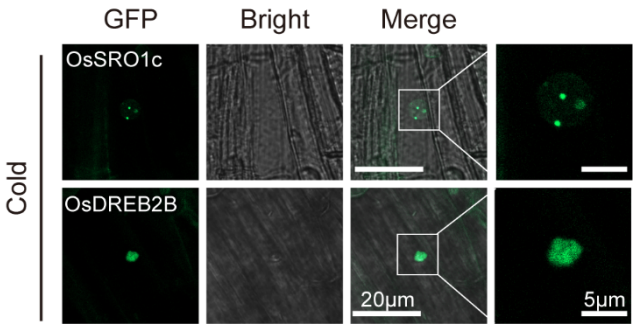

Extended Data Fig. 9 Localization of OsSRO1c^{Hap1} and OsDREB2B in rice root-tip cells after cold stress.

OsSRO1c^{Hap1} and OsDREB2B protein signal (puncta or diffuse) in rice root-tip nuclei after cold stress, respectively. Scale bars, 20 μm (left), 5 μm (right).

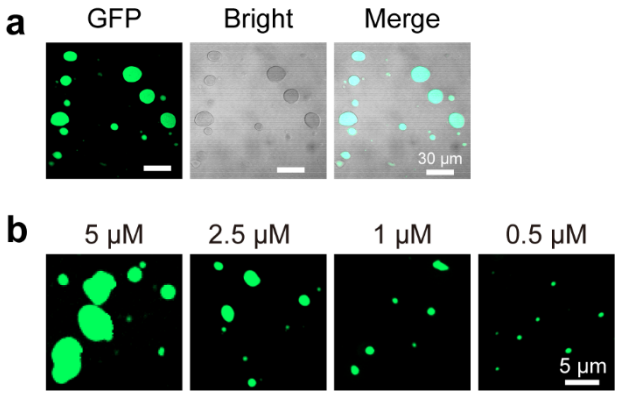

Extended Data Fig. 10 Purified OsSRO1c proteins form liquid droplets *in vitro*.

a, Representative images of OsSRO1c-GFP protein droplets *in vitro*. Scale bars, 30 μm.

b, Purified OsSRO1c proteins form liquid droplet at micromolar protein concentrations. Buffer condition: 200 mM NaCl, pH8.0 and 5% PEG 6,000. Scale bars, 5 μm.

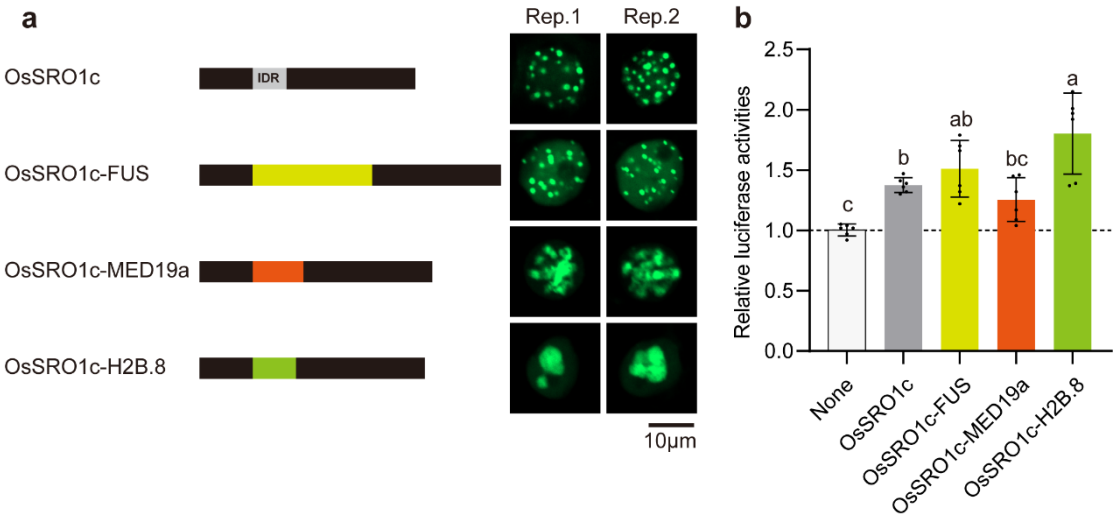

Extended Data Fig. 11 Functional verification of OsSRO1c IDR swapped proteins.

a, Schematic diagrams of IDR swapped vectors (left) and representative fluorescence images of GFP-tagged IDR swapped OsSRO1c protein in tobacco leaves (right). Scale bars, 10 μm.

b, Dual luciferase (LUC) reporter assays of IDR swapped OsSRO1c on transcriptional activity of OsDREB2B under normal conditions. Data represent as mean ± SD. Different lowercase letters indicate a significant difference at the $P < 0.05$ (one-way ANOVA, $n = 6$).

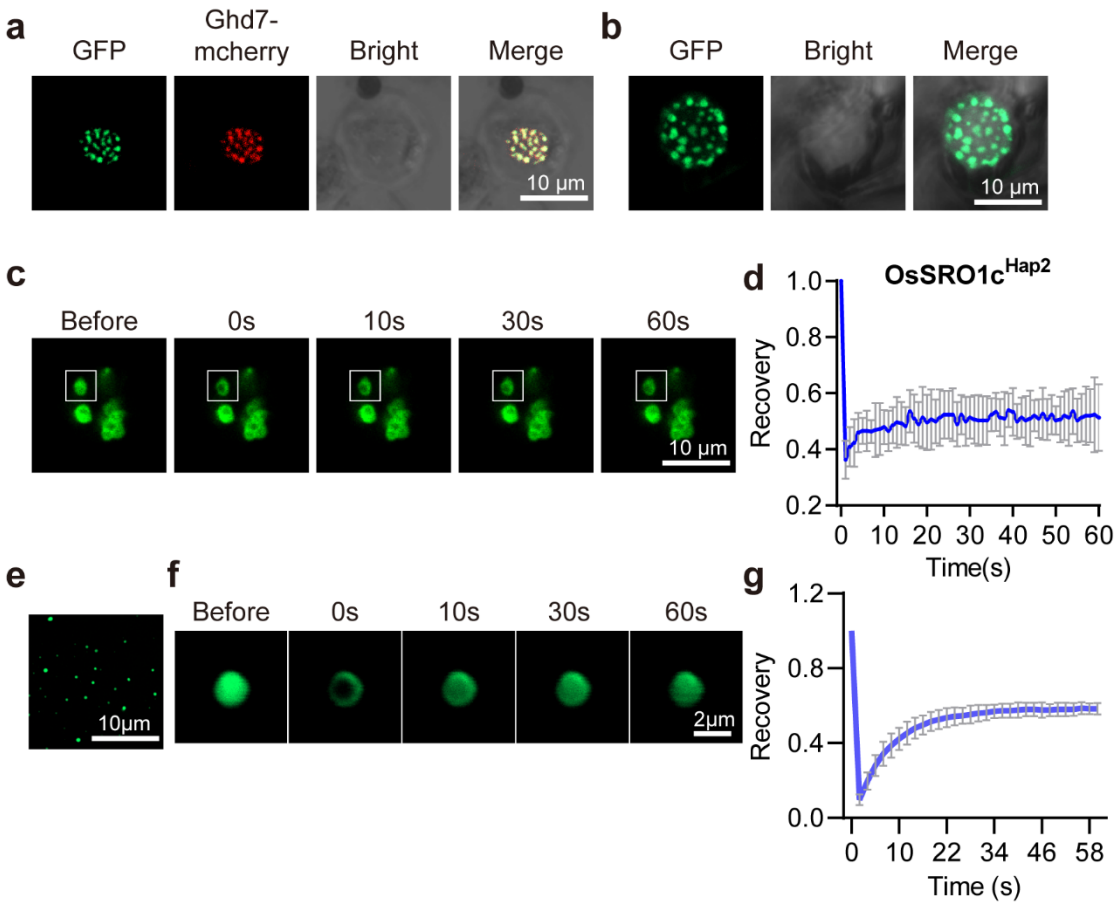

Extended Data Fig. 12 OsSRO1c^{Hap2} undergoes LLPS *in vivo* and *in vitro*.

a. Localization of OsSRO1c^{Hap2} in rice protoplasts under normal condition. Ghd7-mCherry was used as a marker for nuclear localization. Scale bars, 10 μm.

b. Localization of OsSRO1c^{Hap2} in tobacco leaves under normal condition. Scale bars, 10 μm.

c. Representative FRAP images of OsSRO1c^{Hap2} in tobacco leaves. White squares indicate bleached granules. Scale bars, 10 μm.

d. FRAP recovery curve of OsSRO1c^{Hap2} in tobacco leaves. Data represent as mean ± SD (n = 3).

e. The representative images of GFP-OsSRO1c^{Hap2} protein formed LLPS *in vitro*. Scale bars, 10 μm.

f & g. Representative FRAP images (f) and recovery curve (g) of GFP-OsSRO1c^{Hap2} protein *in vitro*. Scale bars, 2 μm. Data represent as mean ± SD (n = 3).

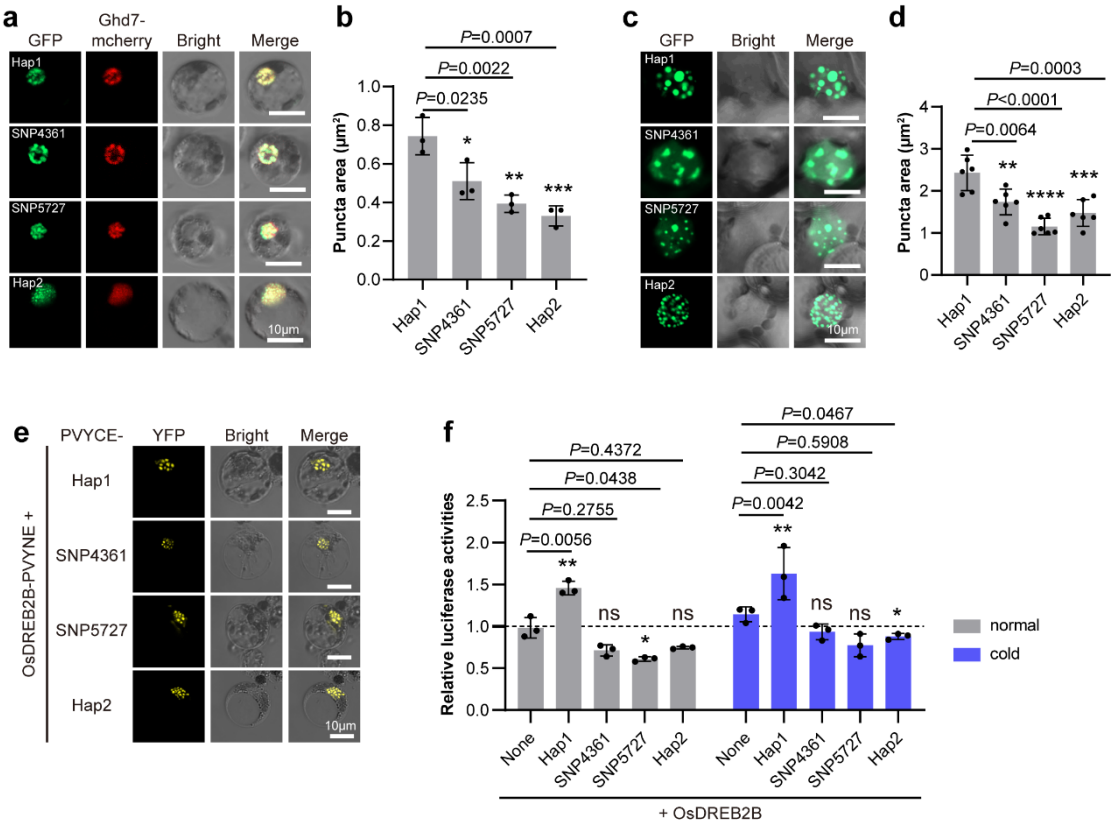

Extended Data Fig. 13 Both natural variations are essential for the function of OsSRO1c

a, Subcellular localization of natural variation of OsSRO1c in rice protoplasts under normal conditions. Scale bars, 10 μm.

b, The average puncta area (μm^2) of OsSRO1c SNP variation in rice protoplasts under normal conditions. Data represent as mean ± SD. (n = 3). Asterisks represent significant differences compared with Hap1 by one-way ANOVA (* P < 0.05, ** P < 0.01, *** P < 0.001).

c, Subcellular localization of natural variation of OsSRO1c in tobacco leaves under normal conditions. Scale bars, 10 μm.

d, The average puncta area (μm^2) of OsSRO1c SNP variation in tobacco leaves under normal conditions. Data represent as mean ± SD. (n = 6). Asterisks represent significant differences compared with Hap1 by one-way ANOVA (** P < 0.01, *** P < 0.001, **** P < 0.0001).

e, Representative BiFC images of OsSRO1c SNP variation interacting with OsDREB2B in rice protoplasts under normal conditions. Scale bars, 10 μm.

f, Effects of natural variation of OsSRO1c on transcriptional activity of OsDREB2B in rice protoplasts under both normal and cold stress conditions. Data represent as mean ± SD. (n = 3). Asterisks represent significant differences compared with None by one-way ANOVA (* $P < 0.05$, ** $P < 0.01$, ns, no significant).

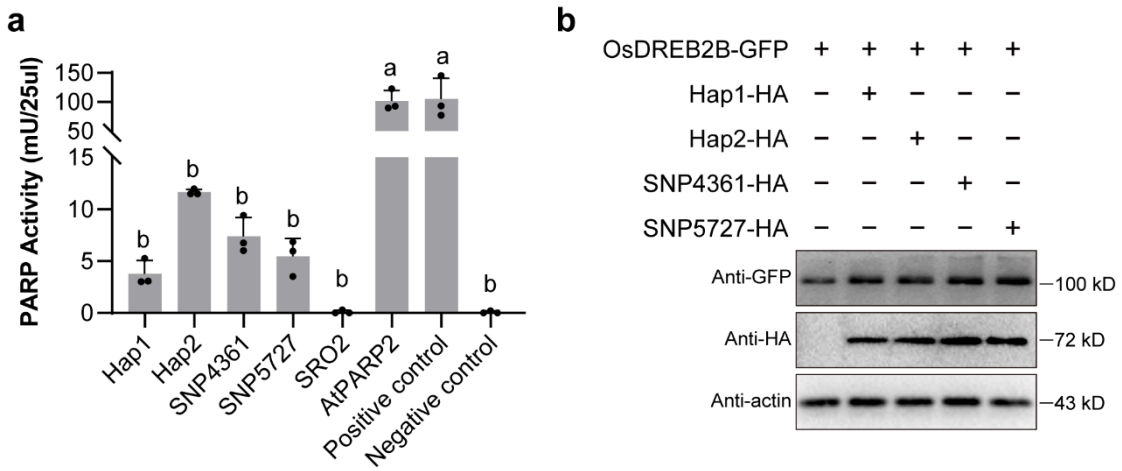

1405

1406 **Extended Data Fig. 14 Biological function detection of natural variation in**

1407 **OsSRO1c.**

1408 **a**, PARP activity assay for different OsSRO1c protein variants. Equal amounts of

1409 purified His-OsSRO1c protein variants (Hap1, Hap2, SNP4361 and SNP5727), His-

1410 SRO2 and His-AtPARP2 proteins were used in the assay. PARP-HSA Enzyme and

1411 PARP Buffer in the kit was used as positive and negative controls, respectively.

1412 Reported SRO2 and AtPARP2 were also used for reference. Data represent as mean ±

1413 SD (n = 3). Different lowercase letters above bars indicate a significant difference at

1414 the $P < 0.05$ level by one-way ANOVA.

1415 **b**, Protein stability detection of OsDREB2B by OsSRO1c variants. OsDREB2B-GFP

1416 alone or OsDREB2B-GFP and OsSRO1c variants co-transform rice protoplasts, and

1417 the GFP antibody is used to detect the protein levels of OsDREB2B-GFP, HA antibody

1418 is used to detect the protein levels of OsSRO1c^{Haps}-HA and plant specific actin antibody

1419 is used to evaluate the equal sample loading.

1420

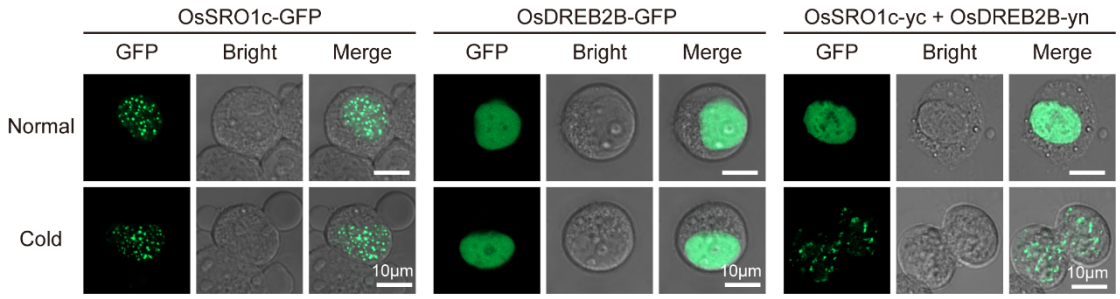

Extended Data Fig. 15 OsSRO1c-OsDREB2B complex responds cold stress in mammalian cells.

Representative fluorescence images of GFP-tagged OsSRO1c (OsSRO1c-GFP) and OsDREB2B (OsDREB2B-GFP) proteins, VC155-tagged OsSRO1c (OsSRO1c-yc) and VN173-tagged OsDREB2B (OsDREB2B-yn) proteins in HEK293T cells. Cells were observed under room temperature (normal) or after treated at 4°C (cold) for 2 h. Scale bars, 10 μm.

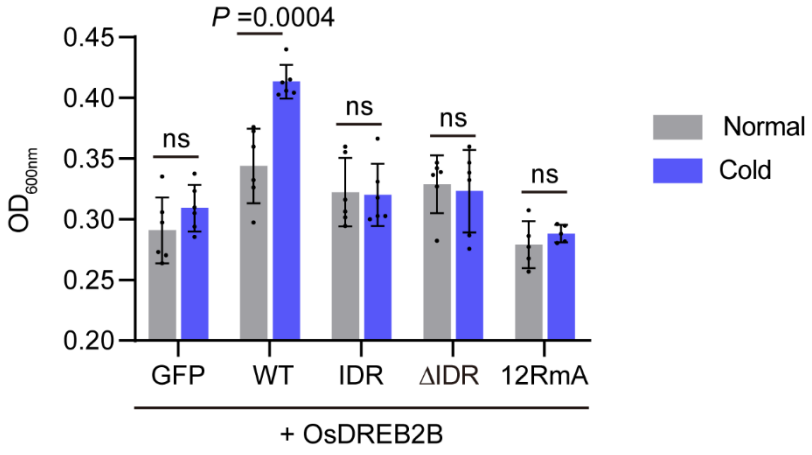

Extended Data Fig. 16 Turbidity measurement of OsSRO1c variants-OsDREB2B complex under both normal and cold stress conditions.

Turbidity measurement of OsSRO1c variants (IDR, ΔIDR, and 12RmA)-OsDREB2B complex under both normal and cold stress conditions (4℃, 2 h). GFP-OsDREB2B was used as a negative control. Data represent as mean ± SD (one-way ANOVA, *n* = 6).

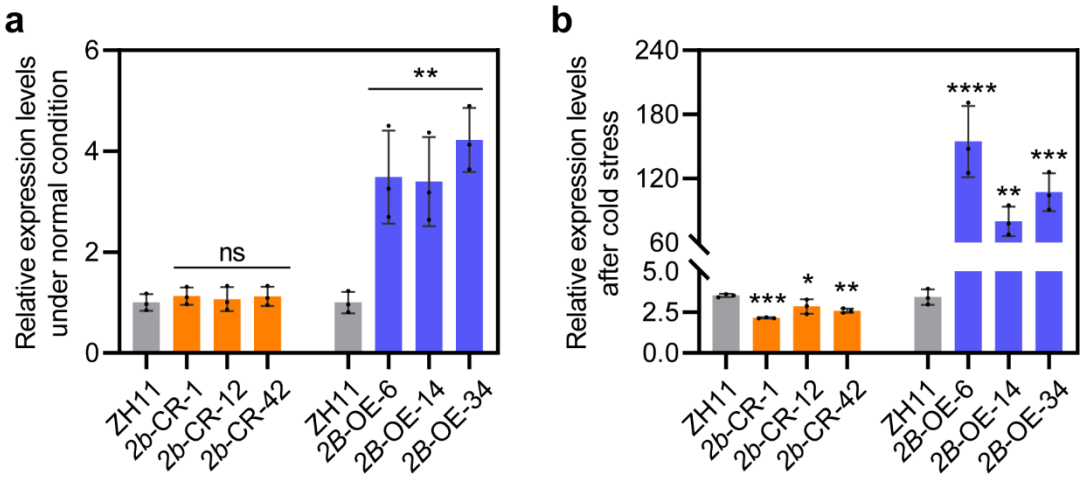

Extended Data Fig. 17 The relative expression levels of *OsSRO1c* in *OsDREB2B* transgenic plants under both normal and cold stress conditions.

a,b The relative expression levels of *OsSRO1c* in ZH11, three *osdreb2b* mutant lines (*2b*-CR-1, *2b*-CR-10 and *2b*-CR-42) and three *OsDREB2B* overexpression lines (*2B*-OE-6, *2B*-OE-14 and *2B*-OE-34) under normal (**a**) and cold stress (**b**). Data represent as mean ± SD (n = 3). Asterisks represent significant differences compared with ZH11 by one-way ANOVA (* $P < 0.05$, ** $P < 0.01$, *** $P < 0.001$, **** $P < 0.0001$, ns, no significant).

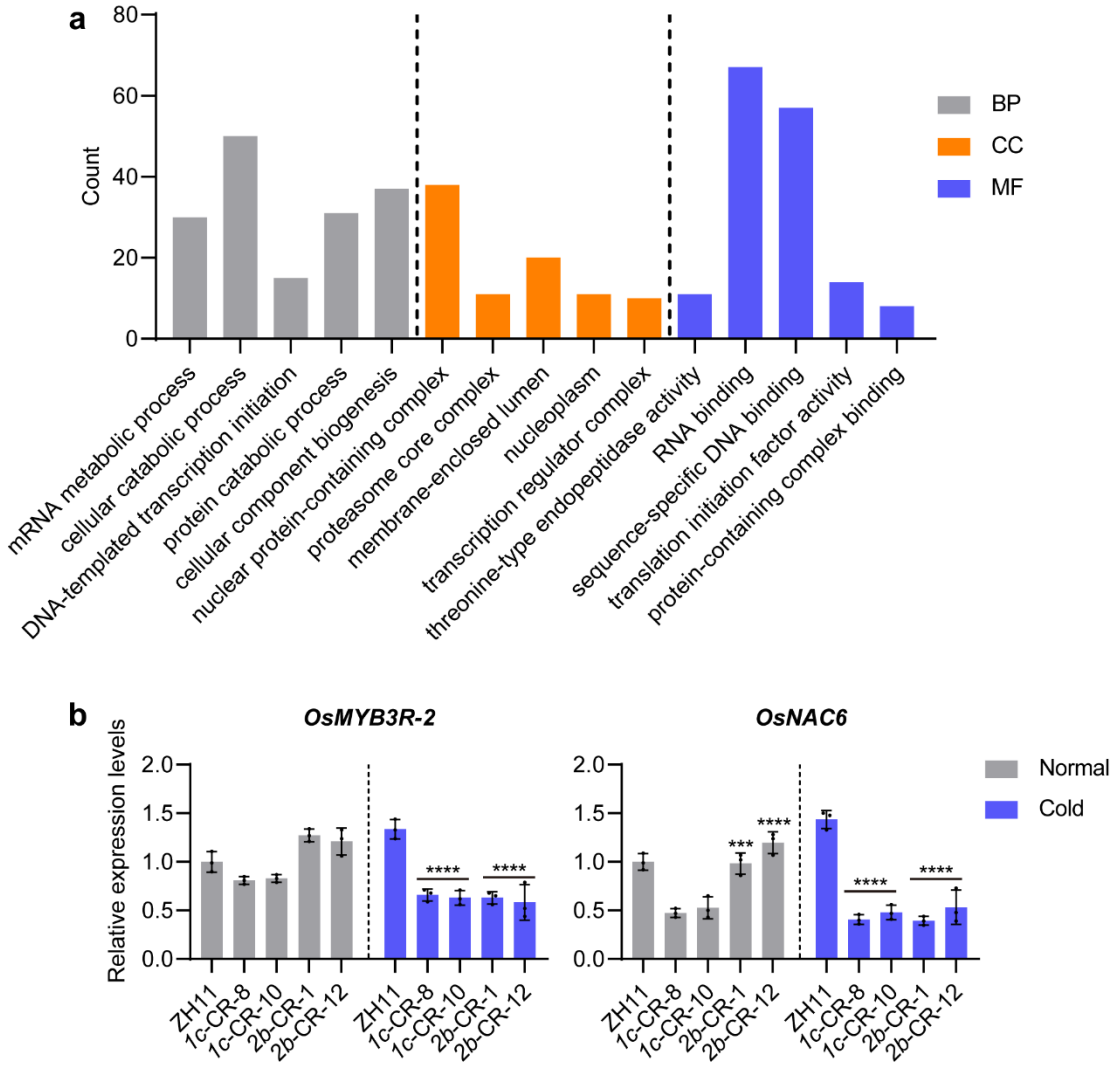

Extended Data Fig. 18 GO analysis of DEGs in RNA-seq and the relative expression levels of well-known cold response genes.

a, GO analysis of co-downregulated genes in both *1c*-CR and *2b*-CR under cold stress. **b,** The relative expression levels of *OsMYB3R-2* and *OsNAC6* in ZH11, *ossro1c* mutants (*1c*-CR-8 and *1c*-CR-10) and *osdreb2b* mutants (*2b*-CR-1 and *2b*-CR-12) under both normal and cold stress conditions. Data represent as mean ± SD (n = 3). Asterisks represent significant differences compared with ZH11 by one-way ANOVA (*** $P < 0.001$, **** $P < 0.0001$).

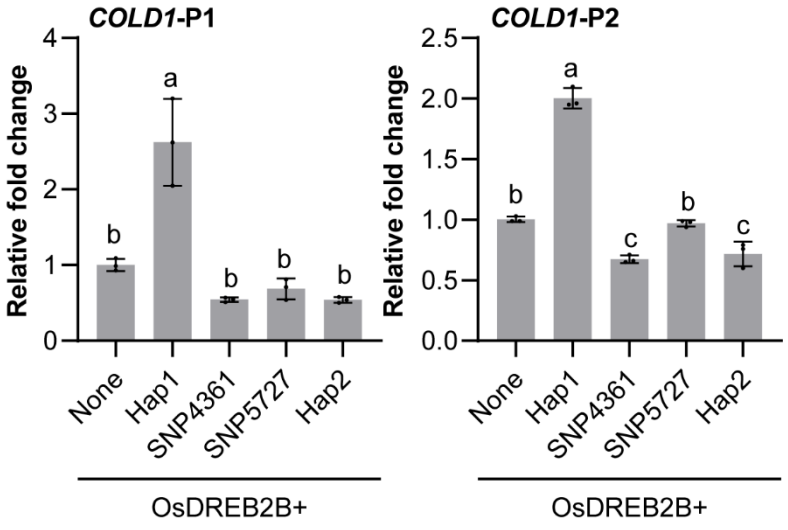

Extended Data Fig. 19 The effect of OsSRO1c variants on the DNA binding ability of OsDREB2B.

ChIP-qPCR assay for effect of OsSRO1c natural variation on OsDREB2B binds to the promoter of *COLD1 in vivo*. Immunoprecipitation was performed with anti-GFP antibody. qPCR enrichment was calculated by normalizing to the None empty vector transformation. Data represent as mean ± SD (n = 3). Different lowercase letters above bars indicate a significant difference at the $P < 0.05$ level by one-way ANOVA.

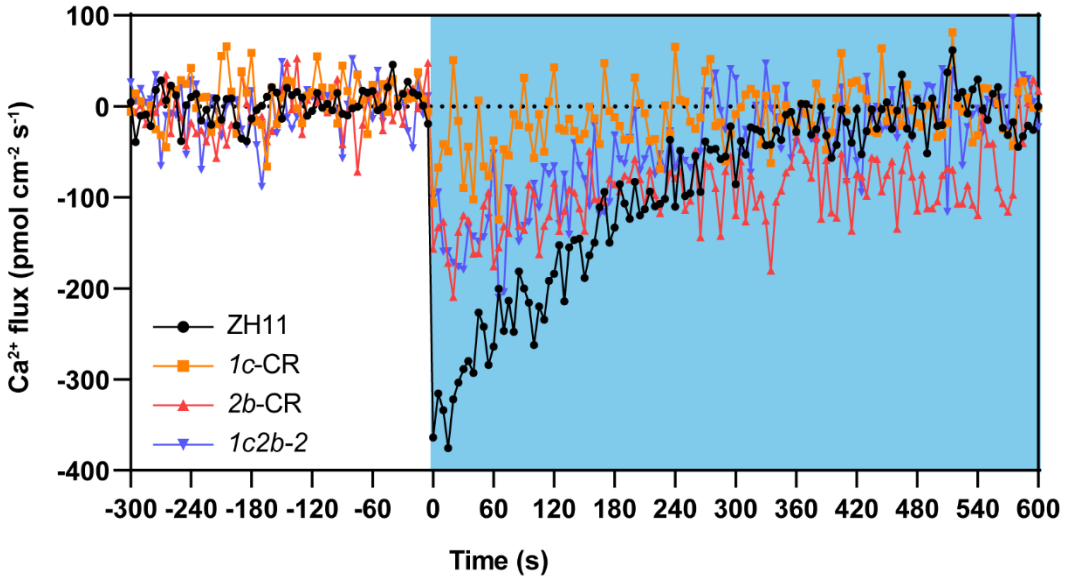

Extended Data Fig. 20 Ca^{2+} Signaling upon cold stress in *ossro1c osdreb2b* mutant lines.

Comparison of Ca^{2+} influx in live roots of ZH11, *ossro1c* mutant (*1c*-CR), *osdreb2b* mutant (*2b*-CR) and *ossro1cosdreb2b double mutant* (*1c2b*-2) upon cold stress.($n > 6$ biological replicates).